12-2014

Refraction Microtremor Analysis of Areas Surrounding California State University San Bernardino

Malcolm D. Thomas
California State University - San Bernardino, malcolm.david.thomas@gmail.com

Refraction Microtremor Analysis of Areas Surrounding California State University San Bernardino

---

A Thesis

Presented to the

Faculty of

California State University,

San Bernardino

In Partial Fulfillment

of the Requirements for the Degree

Master of Science

in

Earth and Environmental Sciences

---

by

Malcolm David Thomas

December 2014

Refraction Microtremor Analysis of Areas Surrounding California State University San Bernardino

---

A Thesis

Presented to the

Faculty of

California State University,

San Bernardino

---

by

Malcolm David Thomas

December 2014

Approved by:

Joan E. Fryxell, Committee Chair, Geology

Jascha Polet, Committee Member

Louis Klonsky, Committee Member

ABSTRACT

The San Andreas Fault stretches for over 800 miles through California. Along the foothills of the San Bernardino Mountains, areas in close proximity to the San Andreas Fault Zone may be subject to site amplification of ground motion caused by seismic activity via wave propagation through the subsurface. These seismic hazards are being addressed via the Alquist-Priolo Earthquake Faulting Zone Act and the National Earthquake Hazards Reduction Program (NEHRP). Shear wave velocity of the subsurface has served as a proxy for ground motion amplification and is therefore a useful parameter to help analyze and reduce seismic hazards. Low shear wave velocities of the subsurface have been known to correlate with higher amplitude ground motion. This study focuses on refraction microtremor analysis (ReMi) of the subsurface in Northern San Bernardino; more specifically, areas encompassing California State University San Bernardino, in close proximity to the San Andreas Fault. The technique will resolve shear wave velocity values for the top 30 meters (Vs30) of the subsurface. This depth of investigation has proven to be an effective means in determining subsurface conditions. ReMi profiles were situated 0.25 to 2.0 miles away from the San Andreas Fault, and in some instances, strategically positioned next to housing developments and structures. Phase velocity dispersion curves were generated by processing ReMi seismic data and subsequently inverted to attain average shear wave velocity profiles with depth. The geologic units in the study area consist of very young wash deposits, young

alluvial fan deposits and Pelonist schist deposits. These geologic units may be an indicator to how seismic waves behave in subsurface lithology. To highlight differences in Vs30 values across the project area, a microzonation map was constructed.

ACKNOWLEDGEMENTS

First and foremost thank you Jesus for allowing me to get this far, I am a product of your will and mercy. Thank you Prof. Polet, for granting me access to the California State Polytechnic University, Pomona departmental equipment for the duration of my fieldwork. To Louis Klonsky, who was instrumental in sparking the idea that I could be a geophysicist, and for being there these past couple of years doing all he could to bring my dreams to fruition, I cannot thank you enough. Thank you Prof. Fryxell for the letters of recommendations and academic guidance you have given me throughout my tenure at California State University, San Bernardino. To Hannah Mejiah, Terry Cheiffetz and all the students at California State Polytechnic University, Pomona for their assistance in completing my field research, without you all I wouldn't have gotten far. Thank you Mom, for having unwavering faith in me, the road has been long and hard but we finally made it. Thank you Jamar, my brother, you provided support and motivation to get to this point. Thank you Aurora for being by my side through this journey. Last but not least, thank you Cal State University San Bernardino and my home away from home California State Polytechnic University, Pomona.

TABLE OF CONTENTS

ABSTRACT iii

ACKNOWLEDGEMENTS v

LIST OF TABLES viii

LIST OF FIGURES ix

CHAPTER ONE: RESEARCH STATEMENT

Introduction 1

Motivations 4

Research Objectives 8

CHAPTER TWO: METHODOLOGY

Background 10

Determination of Shear Wave Velocity 11

Point Source Methods 11

Cross-Well Seismic 13

SASW Technique 15

MASW Technique 16

Sustained Seismic Source Methods 18

ReMi Technique 18

Synopsis 23

Amplification 24

CHAPTER THREE: PROJECT AREA

Geologic Units 26

Local Faults 28
San Andreas Fault Zone 29
San Andreas Fault: San Bernardino Mountains Segment 30
San Jacinto Fault 32
Mill Creek Fault 32
Areas of Interest 33
CHAPTER FOUR: EXPERIMENTAL DESIGN
Project Set-Up 34
Experiment Area Identification 40
Data Collection 42
CHAPTER FIVE: DATA PROCESSING
Field Record Conversion 45
Velocity Model Construction 59
CHAPTER SIX: RESULTS
Data Collection 61
Data Interpretation 74
CHAPTER SEVEN: CONCLUSIONS
Lessons Learned 84
Work for the Future 85
REFERENCES CITED 87

LIST OF TABLES

Table 1. NEHRP SITE CLASSIFICATIONS 7

Table 2. ZONE ONE PROFILE DATA 62

Table 3. ZONE TWO PROFILE DATA 67

Table 4. ZONE THREE PROFILE DATA 71

LIST OF FIGURES

Figure 1. Loma Prieta Seismic Recordings 3

Figure 2. Map Overview of Project Area 8

Figure 3. Horizontal Impulse Schematic 13

Figure 4. Cross-well Seismic 14

Figure 5. SASW Schematic 16

Figure 6. MASW Schematic 17

Figure 7. Field Seismogram 20

Figure 8. Pre-Stack p-f Spectrum 21

Figure 9. Post-Stack p-f Spectrum 22

Figure 10. Example Dispersion Curve 23

Figure 11. San Bernardino Geologic Map 27

Figure 12. Project Overview Map 28

Figure 13. Fault Map 31

Figure 14. Geophones 36

Figure 15. Receiver Cables 37

Figure 16. Data Logger 38

Figure 17. Data Logger Battery 39

Figure 18. Field Array 40

Figure 19. Zones of investigation 41

Figure 20. Geophone Resistance Check 43

Figure 21. Field Record Conversion 48

Figure 22. Specification of Inputs 49
Figure 23. Record Inspection 50
Figure 24. Plot Parameters 51
Figure 25. Pre-Processing 52
Figure 26. Geometry Input 53
Figure 27. p-f Specification Window 54
Figure 28. Example p-f Spectrum 55
Figure 29. Selection of p-f planes 56
Figure 30. Stacked Records with Picks 57
Figure 31. Saving Picks 58
Figure 32. Dispersion Curve and Velocity Model 60
Figure 33. Zone 1 62
Figure 34. Zone 1 Profile One p-f Spectrum 63
Figure 35. Zone 1 Profile One Dispersion Curve 64
Figure 36. Zone 1 Profile One Velocity Model 65
Figure 37. Zone 2 66
Figure 38. Zone 2 Profile Three p-f Spectrum 67
Figure 39. Zone 2 Profile Three Dispersion Curve 68
Figure 40. Zone 2 Profile 3 Velocity Model 69
Figure 41. Zone 3 70
Figure 42. Zone 3 Profile Two p-f Spectrum 72
Figure 43. Zone 3 Profile Two Dispersion Curve 73

Figure 44. Zone 3 Profile Two Velocity Model 74

Figure 45. Vs30 Geologic Unit Correlation Map 75

Figure 46. Geologic Unit Frequency 76

Figure 47. Vs30 Range 78

Figure 48. Cumulative Frequency Plot 79

Figure 49. Qyf_5 Cumulative Frequency 80

Figure 50. Qya_3 Cumulative Frequency 81

Figure 51. Microzonation Contour Map 83

CHAPTER ONE

RESEARCH STATEMENT

Introduction

The refraction microtremor (ReMi) method is an effective geophysical tool. With the utilization of a standard refraction system, one is able to determine shallow shear wave velocities for the underlying shallow subsurface. It has become an important tool for analyzing amplification of ground motion caused by seismic activity, such as during an earthquake, via wave propagation through the subsurface. Such an event can cause significant damage at considerable distances from the epicenter of an earthquake. Likewise, earthquake preparation practices rely heavily on identifying areas of potential hazard, thus bringing to the public's attention a need for enforceable codes and standards when considering the construction of buildings (industrial or residential). Loosely consolidated shallow stratigraphic layers within the subsurface are of primary concern due to their tendency to amplify ground motion. Catastrophic events such as the San Francisco earthquake of 1906 and Loma Prieta earthquake of 1989, where site response played a major role in unexpected destruction, are examples of issues seismic hazards present (Borcherdt, 1975).

Average shear wave velocity for the first 30 meters of the subsurface is known as "Vs30". These shear wave velocity values correlate to site amplification of ground motion. Depending upon the composition of the

subsurface, shear wave velocity and site amplification will have different values and effects given equivalent seismic stimulus. Figure 1 depicts data recorded at several seismograph stations during a magnitude 3.6 aftershock of the Loma Prieta earthquake. Five stations in total, located at sites of differing subsurface composition, recorded ground velocity. Stations BEA and LMS reside in an area where a portion of the subsurface was composed of loosely consolidated hydraulic fill, NPT resides on a loosely consolidated soil, and MAS and CAL were located on top of a sandstone outcrop (O'Rourke, 1992).

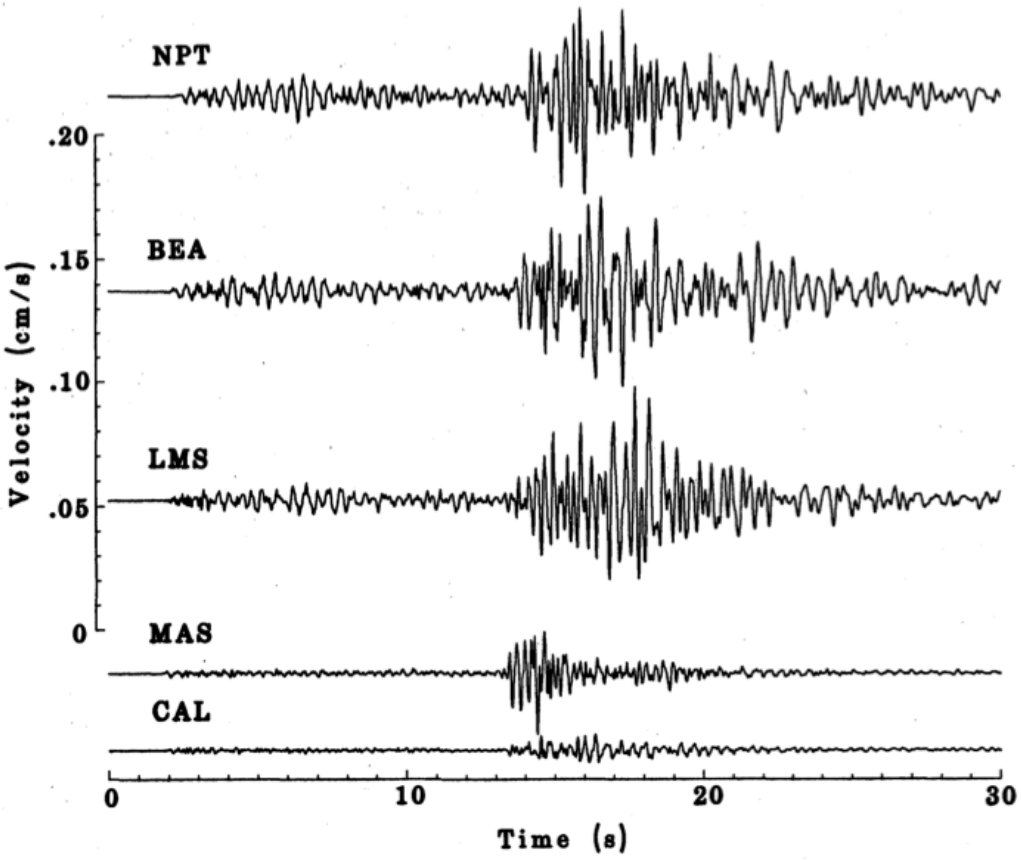

Figure 1. Loma Prieta seismic station recordings showing ground motion velocity from a magnitude 3.6 aftershock recorded at 5 different seismic stations (NPT, BEA, LMS, MAS, CAL) in the Marina District of northern San Francisco. The abbreviations used for the seismic stations are taken from the street on which they are located. For example, BEA is located on Beach Street. The X-axis is time in seconds and the Y-axis represents velocity in centimeters per second (O'Rourke, 1992).

Many methods have been used to study the propagation of seismic waves through the subsurface in an area, although several caveats are noteworthy. These include: costs, space limitations due to restricted areas of deployment, negative public sentiments in urban environments where loud sources are required to generate the seismic wave arrivals needed for data acquisition and

the potential difficulty to identify the requisite shallow Raleigh surface waves due to excessive noise generated by automobile traffic or heavy machinery. These methods and shortcomings are explained further in the subsequent chapter. Caveats aside, the ReMi method has proven to be an effective technique for gathering seismic wave data, while remaining cost and time efficient, and urban environment friendly. Most important, it has proven to be viable for examining shallow Raleigh surface wave propagation ultimately allowing for the identification of shear wave velocities in the subsurface.

The process of using microtremor phase velocities to determine shear wave velocities is a relatively old method (Aki, 1957, as cited by Horike, 1985). Aki was one of the first investigators to deduce the vertical and horizontal phase velocity components of microtremors, enabling the identification of Shear wave velocity structure at 3 meters in depth (Horike, 1985). In contrast, the use of the refraction microtremor method for seismic hazard assessments is a fairly recent application.

Motivations

Motivations behind identifying tools to assess geologic hazard due to earthquake events include the devastating California earthquake of 1906, which led to the destruction of a significant portion of the San Francisco Bay area, causing over $400 million dollars in damages and the deaths of an estimated 700 inhabitants (Borcherdt, 1975). The cause of the disaster was primarily attributed to the geologic condition of the subsurface, which was primarily composed of

loosely consolidated sediment upon which bay communities were built upon. The rupture of the northern segment of the San Andreas Fault was the origin of the seismic event. After this incident, efforts were made, such as those identified in Lawson et al. (1969), to determine the position of the San Andreas Fault. This led to the mapping of the fault from San Francisco, in Northern California, through Los Angeles, in Southern California (Lawson et al., 1969). This work was one of the first investigative measures to identify major faults in Southern California and highlight potential geologic hazards. Another significant seismic event that focused widespread attention on the need for national earthquake hazard zonation standards was the Loma Prieta earthquake of 1989. The M7.1 earthquake originated along the northern stretch of the San Andreas Fault in the Santa Cruz Mountain region (Segall, 1990). The Loma Prieta earthquake, along with the Northridge earthquake in 1994 generated a consensus by the U.S. government, for the need of new provisions to the Earthquake Hazards Reduction Act, which were recommended by the National Earthquake Hazards Reduction Program (NEHRP) in 1997. These provisions include regulations for new structures (Stewart and Liu, 2000). For example, the new regulations highlight specific materials that should be used or not used within structures to prevent structural failure during a seismic event.

In 1977 the United States Congress passed the Earthquake Hazards Reduction Act and in the same year the act mandated NEHRP. The goals of NEHRP are to provide applicable standards regarding earthquake damage

prevention, deliver the latest methods to decrease loss due to earthquake hazard susceptibilities, enable proficient earthquake hazard identification, and increase the knowledgebase to better understand the nature of earthquakes and their consequences (Building Seismic Safety Council, 2003). Years since the Acts passing, several provisions have been made to update the law using new information garnered which may help in effectively highlighting earthquake hazards and means to prevent them (FEMA, 1997). In 1997 a provision was added to the Earthquake Hazard Reduction Act, emphasizing the effects of ground motion by detailing ground motion amplification/acceleration scenarios and techniques for analyzing them. In addition, the provision underscores new standards for the construction of buildings and structures by identifying the behavior of materials within failed structures of the past, and provides improvements to structural design for future construction.

Efforts have been made by NEHRP to map shear wave velocity values for the first 30 meters of the subsurface, and the results are published as site classification maps. These maps show average velocity profiles across an area, and allow for the identification of possible high amplification areas classified and ranked by NEHRP. Site classes rank from A-E and are cataloged by rock type and Vs30 as depicted in Table 1. Areas exhibiting large seismic wave amplifications are assumed to be zones with lower Vs30 values i.e., site classes D and E, consisting of stiff and soft soils (Table 1). Such amplification in the subsurface can compromise structures on the surface during seismic activity.

TABLE 1. NEHRP SITE CLASSIFICATIONS

Site Class	Soil Profile Name	Minimum Vs30 (m/s)	Maximum Vs30 (m/s)
A	Hard Rock	>1500	
B	Rock	>760	1500
C	Very Dense Soil and soft rock	>360	760
D	Stiff Soil	180	360
E	Soft Soil		<180

Note: Adapted from Holzer et al., 2005

The Alquist-Priolo Earthquake Fault Zoning Act was signed into California law in 1972 and is designed to reduce human risk through regulating the construction and or location of a structure of occupancy in proximity to active fault zones. Areas that are subject to the legislation are considered “active” fault zones. A fault is deemed active if it has ruptured within the past 11,000 years (Alquist and Priolo, 1972). According to the Alquist-Priolo Act, the reasonable setback distance from an active fault trace is 50 ft. (Alquist and Priolo, 1972).

Regions of investigation are in close proximity to the San Andreas Fault Zone, which runs along the southern margin of the San Bernardino Mountains. They are also in a populous area as shown in Figure 2, encompassing California State University, San Bernardino and several businesses and residential developments. It would be advantageous for the public’s safety to conduct a microzonation study and develop a NEHRP Site Classification map. The

investigation should include a hazard zone report for areas in northern San Bernardino, in an effort to ensure construction quality control, and geologic hazard identification in locales of known faulting.

Figure 2. Map overview of project area, showing a well populated area.

Research Objectives

Principal objectives of the research detailed in this thesis are to identify hazardous zones located on and around the campus of California State University San Bernardino and surrounding communities using the ReMi method. These hazardous zones may be subject to increased ground motion amplification at the surface due to subsurface compositions. This was accomplished using the ReMi method to determine average shear Vs30, leading to the identification of specific site classifications as outlined by the NEHRP. Likewise, a microzonation

map detailing specific site classifications across the project area was constructed to visually depict potential zones of seismic hazard. In total, over 30 shear velocity profiles were obtained. In order to comprehensively understand the implications of the shear wave velocities garnered, the geology of the project area was researched. This included identifying major fault zones and primary geologic units, understanding the depositional environment of the sediments, as well as utilizing ground water well log data to bolster stratigraphic analyses.

CHAPTER TWO

METHODOLOGY

Background

The determination of shear wave velocity is an essential task when identifying potential seismic hazards. This is accomplished by classifying Vs30 values using the seismic hazard metric utilized by the NEHRP as a standard guideline. This metric categorizes average shear wave velocities for the first 30 meters of the subsurface into specific ranges and sediment types. The stress and subsequent motion of the medium, which is subject to seismic wave propagation, are ultimately the main concerns within a site with a poor site classification ranking.

There are two types of seismic waves, body and surface waves. Body waves consist of Primary waves and Shear waves. Primary waves are compressional in nature and shear-waves are longitudinal. Surface waves consist of Rayleigh and Love waves. Rayleigh waves propagate in a rolling modality, having a horizontal component in addition to a shearing component. Love waves have a shearing component in the shallow subsurface. From the identification of the shear wave velocity for the first 30 meters within the subsurface, the calculation of shear stress is partially possible as seen in the following equation.

$$G = \rho V_s^2 \qquad \text{EQ 1}$$

G is defined as the shear modulus; ρ represents density, and Vs represents shear wave velocity. By identifying the density/densities of the subsurface and inputting shear wave velocities for a stratigraphic interval or an average shear wave velocity for an entire depth interval; one is able to deduce the overall ratio of shear stress to shear strain.

Determination of Shear Wave Velocity

There are many methods and approaches that can be utilized when identifying shear wave velocities in soils. These methods have become increasingly important when considering the adverse effects earthquakes yield. Two methods utilized to accomplish these analyses are the impulsive seismic method and sustained source method (Duke, 1969). The impulsive seismic method includes techniques that utilize active impulses delivered from the application of detonated explosive devices or mechanical inputs. These seismic sources are positioned above or below the surface, allowing wave arrivals to be recorded at or below the surface. The body wave procedure, cross well correlation procedure, spectral analysis of surface waves (SASW) technique, and multi-channel analysis of surface waves (MASW) technique are some of the means by which the impulsive seismic method can be applied.

Point Source Methods

The body wave procedure records wave arrivals traveling along a

horizontal plane. Impulses are provided by explosive detonations and mechanical forces to generate body waves. Arrivals are detected using a standard geophone array, with each geophone positioned normal to the surface. For example, a seismic source input would be applied to the side of a shallow trench and geophones orientated in the same direction, as the impulse application would record wave arrivals. Despite the horizontal direction of impulse application, Primary-waves and Shear-waves are generated (Duke, 1969). Shear-wave arrivals are observable on a seismic trace, allowing for the computation of shear wave velocities (Figure 3).

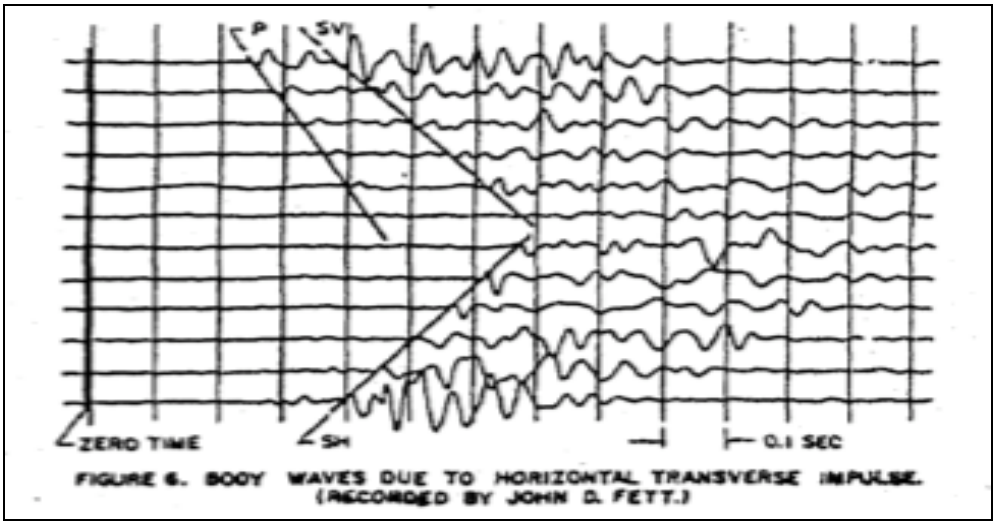

Figure 3. Horizontal wave arrival schematic showing P and S wave arrivals from horizontal impulse, where the x-axis is receiver distance and y-axis is time (Duke, 1969).

Cross-Well Seismic

A more recent point source seismic method utilizes cross-well correlation to determine shear wave velocities i.e., seismic tomography. In essence, a seismic source is placed into a well bore and in another well bore a string of geophone receivers are placed (Figure 4), with an inter-well spacing of no further than 2 km (Hoversten et al., 2004). The seismic waves produced in the first well travel laterally through the subsurface and arrive at the receiver well. Source and receiver wells are no more than 2,000 feet in depth (Hoversten et al., 2004). Alternatively, a string of geophone receivers can be placed in one well, and point seismic sources on the surface. Waves propagating from the surface arrive at the string of receivers at depth. Both schemes give a higher structural resolution

of the subsurface compared to that from a standard surface point source to surface receiver setup, and also allow for the determination of shear wave velocities. The oil industry has utilized these techniques during surveying processes.

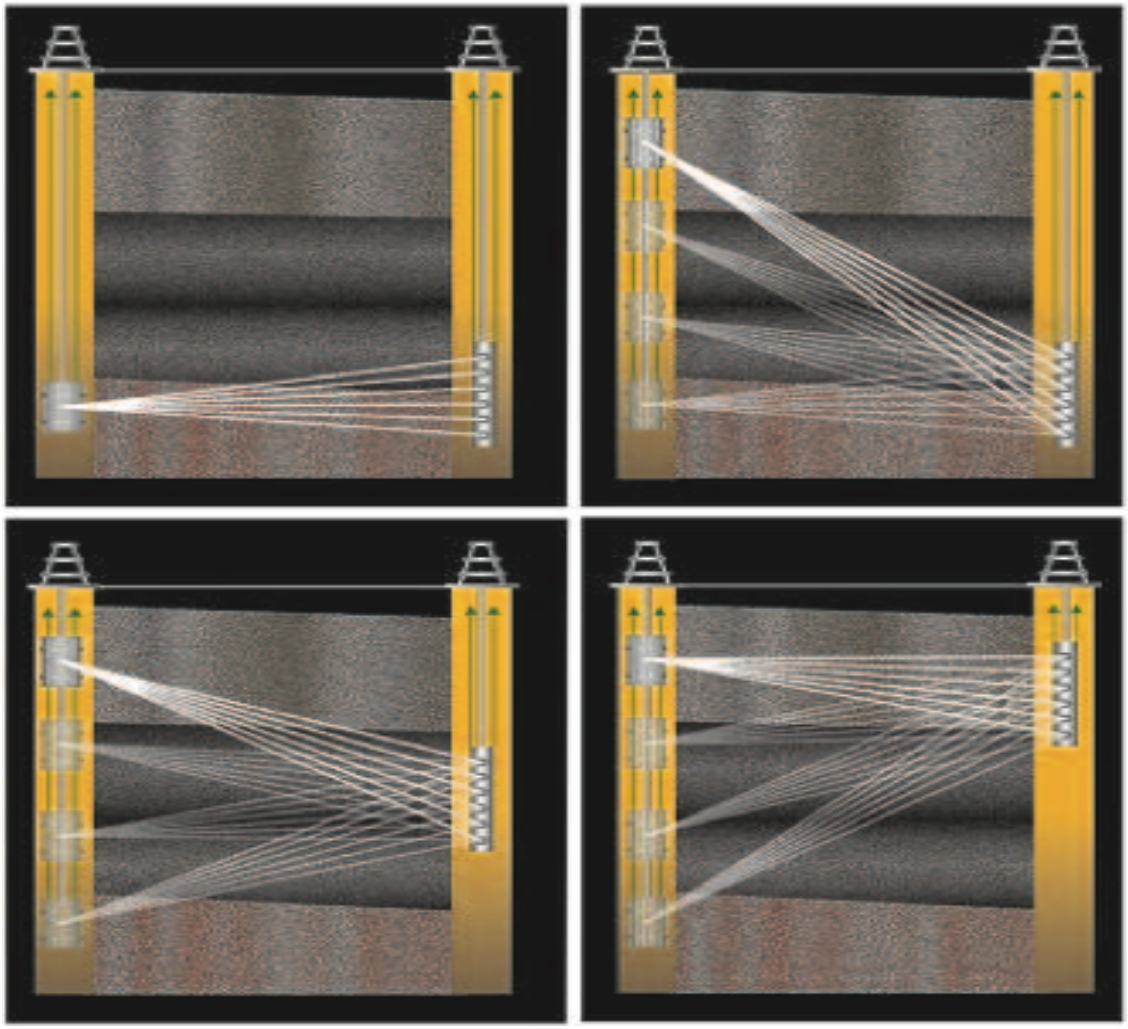

Figure 4. Cross-Well seismic schematic depicting several shot to receiver scenarios (Marion, 2014).

SASW Technique

First proposed by Heisey (1982), the spectral analysis of surface waves (SASW) technique utilizes a two-receiver system, spaced 1 to 500 meters apart, to record ground roll produced by an active source (Figure 5). Spectral analysis of seismic records occurs after data acquisition (Louie, 2001). For more effective data acquisition, multiple frequency ranges can be acquired by adjusting the reception characteristics of the receiver pair. Dispersion curves are created based on the analysis of the frequency domains of the acquired data (Park et al., 1999). This is made possible by analyzing phase differences between acquisition intervals from the pair of receivers, which can be used to determine shear-wave velocities. In summary, shear wave velocity profiles are created by acquiring Rayleigh wave arrivals, allowing for the development of dispersion curves, and the inversion of phase velocity and frequency data to ascertain velocity values. Because this technique focuses on shallow subsurface data acquisition with data quality dependent on the survey environment, the ability to differentiate desirable signal from noise is difficult in noisy areas. These shortcomings are exacerbated because the technique utilizes only two receivers (Park et al., 1999). Boore and Brown (1998) compared shear wave velocity data garnered by the SASW technique to those from borehole measurements at six locations. The SASW technique was found to underestimate shear wave velocities at all 6 sites, ultimately leading to the over estimation of ground motion amplification.

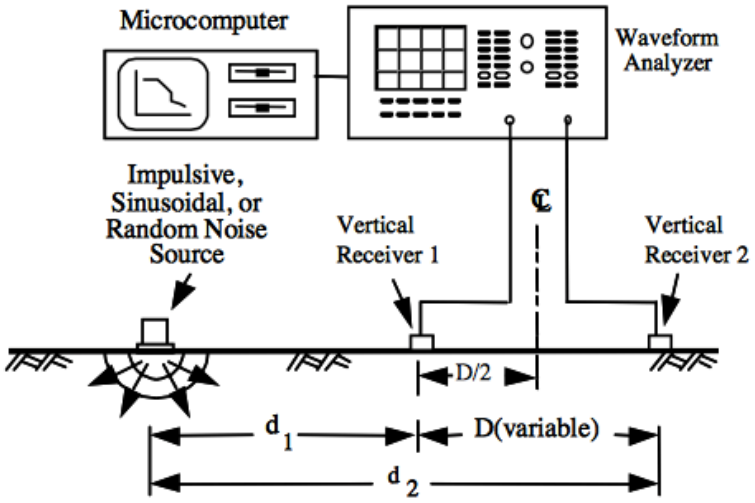

Figure 5. SASW Schematic of a field array layout. D/2 is half the distance between receiver 1 and receiver 2, d_1 is the distance of the seismic source from receiver 1, d_2 is the distance between the seismic source and receiver 2, and D(variable) is the distance between the first and second receiver. A waveform analyzer and microcomputer are used to record wave arrivals (Rosenblad et al., 2002).

MASW Technique

The multichannel analysis of surface waves (MASW) technique is similar to the SASW process, but instead of one pair, utilizes multiple geophone receivers to record wave arrivals to provide enhanced accuracy (Figure 6). The MASW process was designed to overcome the shortcomings of the SASW technique. The process utilizes a standard refraction/reflection geophone array arrangement, where multiple geophones receive wave arrivals. Variations in offset distance and the ability to record multiple seismic records are an advantage (Park et al., 1999). An active source is provided to generate

Rayleigh wave propagation. Time-spatial seismic records are converted to a slowness-frequency domain by analyzing only the shear-wave component of a Rayleigh wave. This is done using a Gaussian transformation. The conversion allows for the formulation of dispersion curves. By analyzing these slowness-frequency dispersion curves, shear wave velocity can be determined (Stephenson et al., 2005). The technique has also been found to effectively resolve Raleigh wave arrivals in noisy environments, thus providing a huge advantage over the SASW method (Louie, 2001).

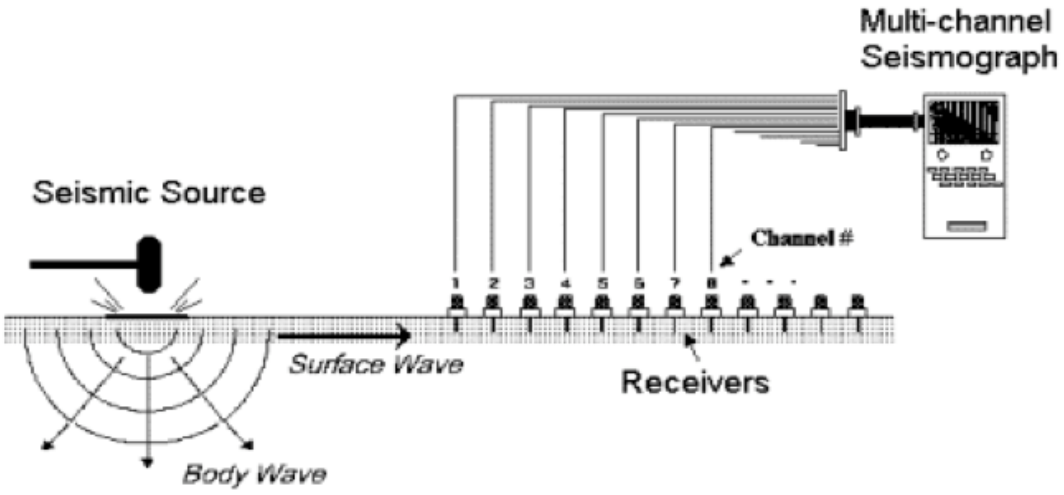

Figure 6. A schematic of the MASW technique, where a point seismic source is represented by a hammer strike, where wave arrivals are recorded by geophones (Park et al., 1997).

Sustained Seismic Source Methods

Continuous seismic source methods allow for the acquisition of seismic wave arrivals and determination of shear wave velocities utilizing a variety of sources. These include, but are not limited to: sustained seismic inputs provided by mechanical vibrations, ambient noise from automobile traffic, heavy machinery, or train locomotion. These sources are “passively” present in the environment and are not directly applied. For example, a Vibroseis truck provides a direct application of a continuous seismic stimulus, whereas cars driving on the freeway provide a passive seismic stimulus. These inputs can be deployed above or just below the surface. Examples of subsurface inputs are subterraneous machinery or large diameter pipes with high volumes of water flowing. The ReMi technique allows for the acquisition of seismic data from passive continuous seismic sources.

ReMi Technique

The ReMi process takes the best of both the SASW and MASW techniques. It utilizes a standard refraction/reflection geophone array to record ground roll in the form of Rayleigh waves from ambient seismic wave sources. These sources are identified from the seismic noise generated from automobile traffic or heavy machinery. Geophone arrays are generally arranged in a linear fashion. The length of the profile and resonant frequency of the geophone

receivers determine the maximum depth of investigation. Typically, half the length of the geophone spread is comparable to the depth of investigation below the surface. Thus, to garner shear wave velocities for the first 30 meters of the subsurface requires a geophone array of at least 60 meters. The technique's maximum depth of effective investigation is approximately 100 meters. This is because the quality of Rayleigh wave data acquisition diminishes with depth. Upon commencing data acquisition, multiple ambient seismic records are recorded, each with a specific duration. For example, for one profile, 12 records may be collected, with each record consisting of 30 seconds of data. The collection of multiple seismic records allows for higher quality data acquisition and ensures the reliability of post-processing calculations.

Once Rayleigh wave arrivals are collected, the seismic data, in the form of seismograms, Figure 7, are transformed from a spatial-time domain to a frequency-slowness (p-f) domain. All records of one profile produce individual p-f spectra (Figure 8). They are then stacked to produce p-f spectrum diagram. The stacking process allows for the quality control of data by normalizing outliers and increasing data and image resolution. Following this step, p-f spectrum diagrams are interpreted. Picks are manually made, using processing software, along the surface wave amplitude curve of the spectrum diagram using specialized computer software (Figure 9). These picks are then inverted to generate a dispersion curve, as shown in Figure 10, representing velocity versus period; average shear wave velocities are then determined (Louie, 2001).

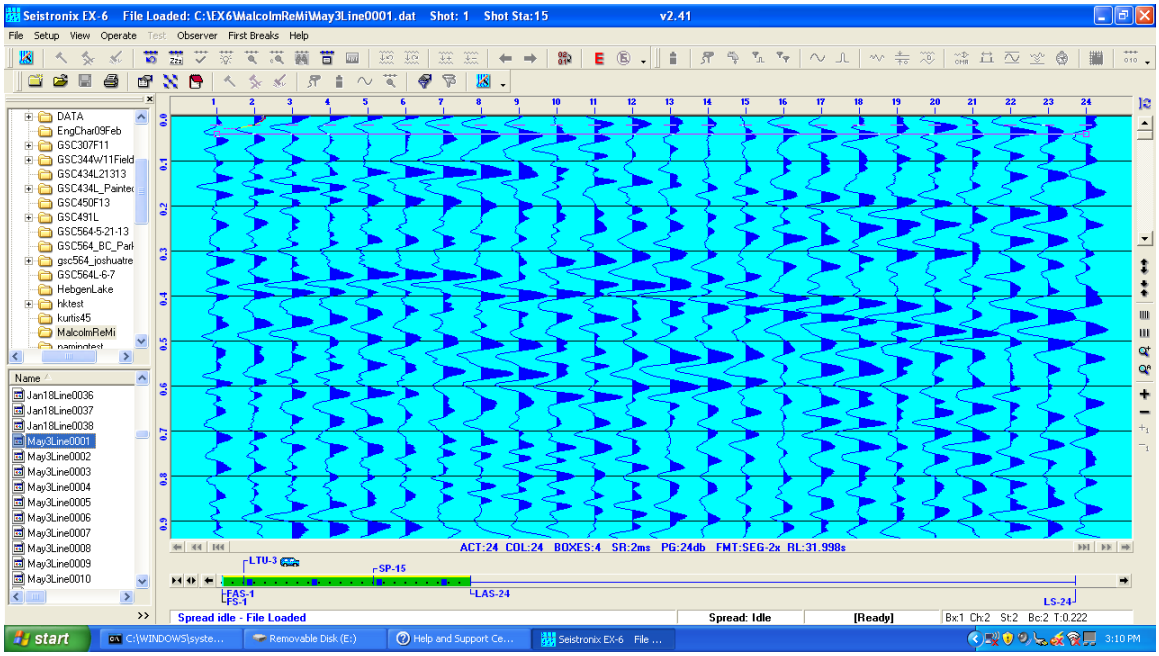

Figure 7. Field seismogram showing wave arrivals, where geophone receivers are at a fixed interval. Geophone spacing is the x-axis and time in m/s is the y-axis.

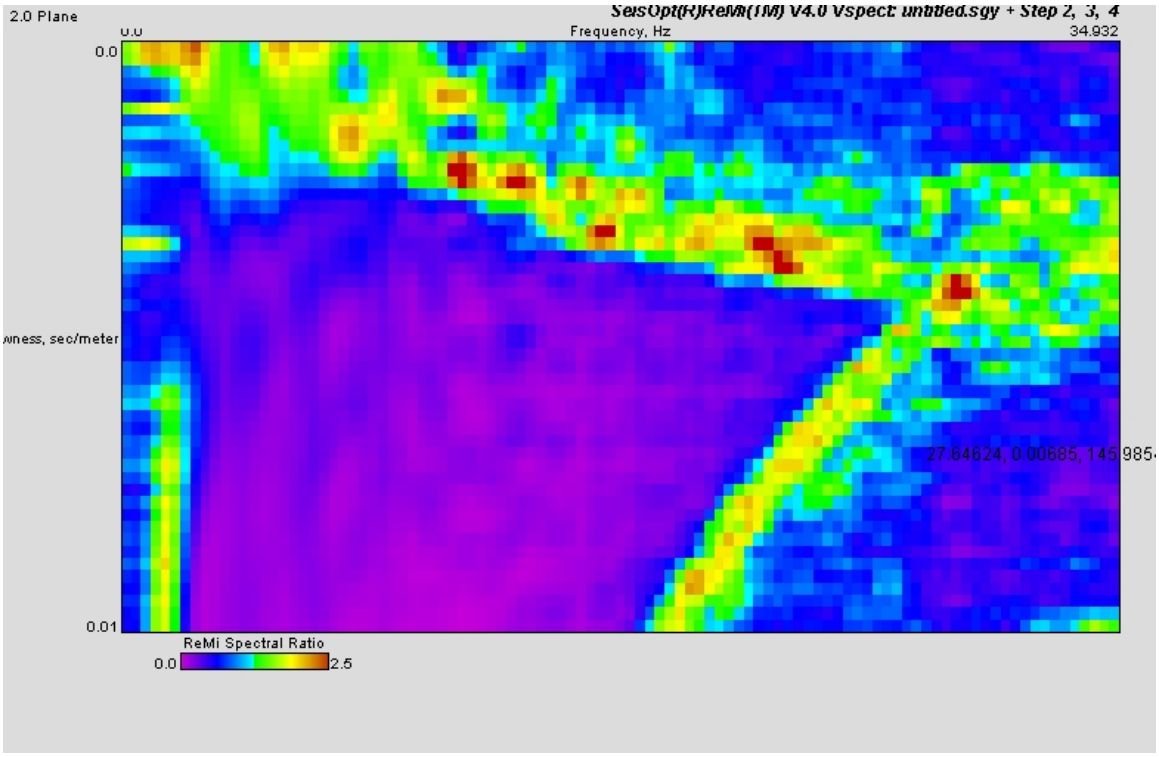

Figure 8. A p-f spectrum for one record out of 12 prior to stacking, where the x-axis is frequency and the y-axis is slowness.

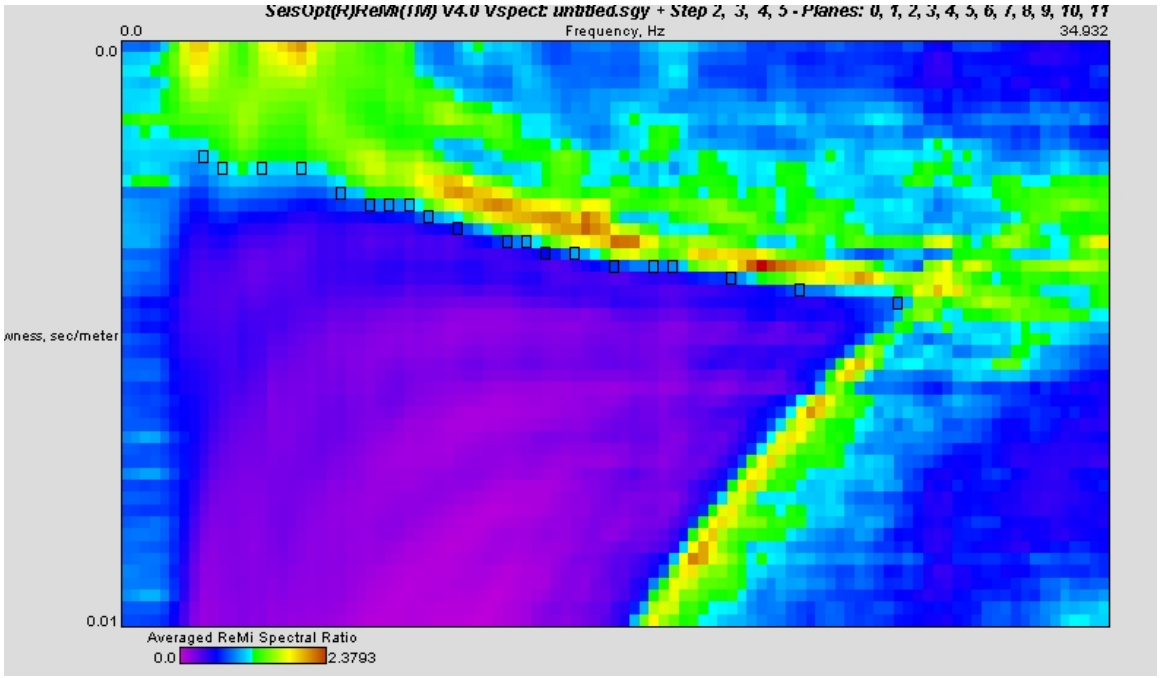

Figure 9. A p-f spectrum image after stacking showing a much smoother image. In addition, picks are identified as black boxes along the high amplitude dispersion trend.

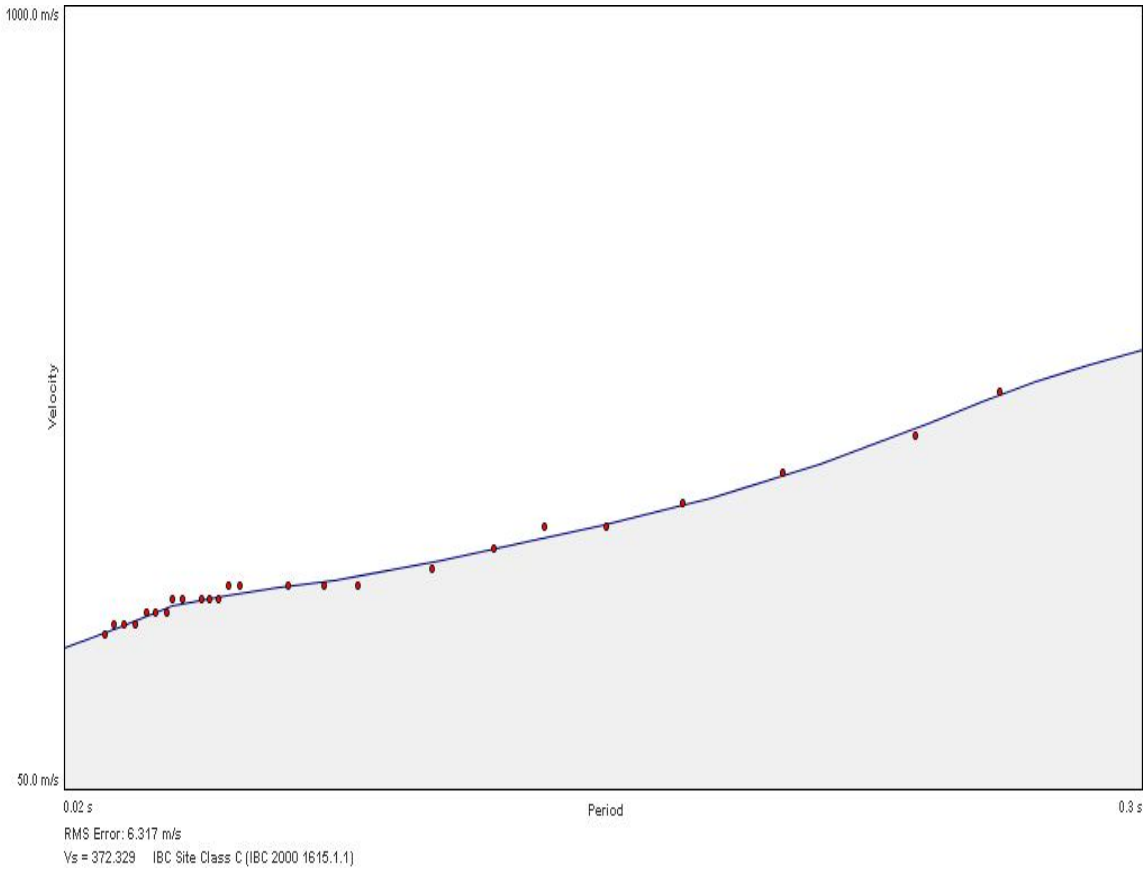

Figure 10. An example dispersion curve generated by inverting picks made along a p-f spectrum. This allows for the determination of shear wave velocity and site classification.

Synopsis

The ReMi approach is similar to the multichannel analysis of surface waves technique. The main advantage of the ReMi technique, compared to the MASW approach, is the lack of a need of an active seismic source. In addition, the ReMi technique allows for the determination of subsurface shear wave velocities in more diverse environments, where the presence of ambient noise is a positive for data acquisition efforts. Another advantage of the ReMi approach

is the quality control phase, where frequency-slowness record stacking occurs. During this step, records containing artifacts due to issues during data acquisition can be manually filtered and discarded, while relevant data can be kept and then stacked for p-f spectrum construction. Ground-roll data recorded using the MASW technique require no pre-processing.

Shortfalls of the ReMi method include the need for ambient seismic noise to produce recordable Rayleigh wave data. If a continuous source of noise is too far away from the geophones, or not strong enough, reliable dispersion curves will not be generated. Additionally, in situations where there is no ambient seismic noise generated, for example the cessation of automobile traffic on a road, no usable data will be acquired. Lastly, because pre-processing steps after data acquisition require data interpretation, resultant data is only as reliable as the interpreter. However, this is generally the case with seismic methods.

Amplification

Site amplification of ground motion is the primary concern of this study. After average shear wave velocities are derived, amplification can be determined. Equation 2 below is used to convert shear wave velocity values to identify amplification factors for specific sites.

$$A = 1/\sqrt{(Vs*\rho)} \qquad \text{EQ 2}$$

A is equal to amplification, Vs, shear velocity and ρ, density (Roser and Gosar, 2010).

As seen, amplification is equal to the inverse of the square root of shear wave velocity multiplied by density. Resultant data provided by the ReMi method does not provide strong restraint for the value of density; consequently, density is treated as a constant. In essence amplification is directly proportional to the inverse of the square root of shear wave velocity. Thus, the higher the shear wave velocity the lower the amplification factor. Likewise, the lower the shear wave velocity the higher the amplification factor. Using the ReMi method, the goal of this study is to define areas based on NEHRP site classifications using shear wave velocity to calculate corresponding site amplification factors that highlight potential ground motion. Finally, correlating these characteristics to corresponding geologic units will help estimate shear wave velocity and amplification factors outside of the project area.

CHAPTER THREE

PROJECT AREA

Geologic Units

Figure 11 depicts the predominant surface geological units of the San Bernardino area. The experiment area is located along the foothills of the San Bernardino Mountains (outlined in blue in Figure 11). The most significant identified units within the area of interest are very young wash deposits (Qw), young alluvial fan deposits unit 1 (Qyf_1), young alluvial fan deposits unit 3 (Qyf_3), young alluvial fan deposits unit 5 (Qyf_5), young alluvial valley deposits unit 3 (Qya_3), and Pelona schist (Mzps), depicted in Figure 11 (Morton and Miller, 2006). The very young wash deposits type, Qw, is young in age (late Holocene), and is composed of unconsolidated to locally cemented deposits of sand and gravel with little to no soil development (Morton and Miller, 2006). The compaction of the unit ranges from unconsolidated to moderately consolidated. Unit 1 alluvial fan deposits (Qyf_1) dates back to the middle Holocene. It is composed of fine to coarse-grained sand in addition to gravel consisting of pebbles and boulders. The compaction of the unit ranges from unconsolidated to moderately consolidated (Morton and Miller, 2006). Unit 3 young alluvial fan deposits (Qyf_3) date back to the middle Holocene. The unit is composed of fine to coarse-grained sand in addition to pebble-boulder gravel, all of which are slightly to moderately consolidated. The unit 5 young alluvial fan group (Qyf_5) is similar in

age (late Holocene), and is composed of fine to coarse-grained sand in addition to a gravel consisting of pebbles and boulders (Morton and Miller, 2006). Unit 3 young alluvial valley deposits (Qya_3) date back to the middle Holocene. The unit is composed of moderately to well consolidated gravelly sand, as well as granule to boulder gravel. Lastly, the Pelona schist (Mzps) unit is of Mesozoic age, and contains feldspar and quartz. The San Andreas Fault crosses what appears to be a contact between alluvial deposits and quartz monzonite (Morton and Miller, 2006).

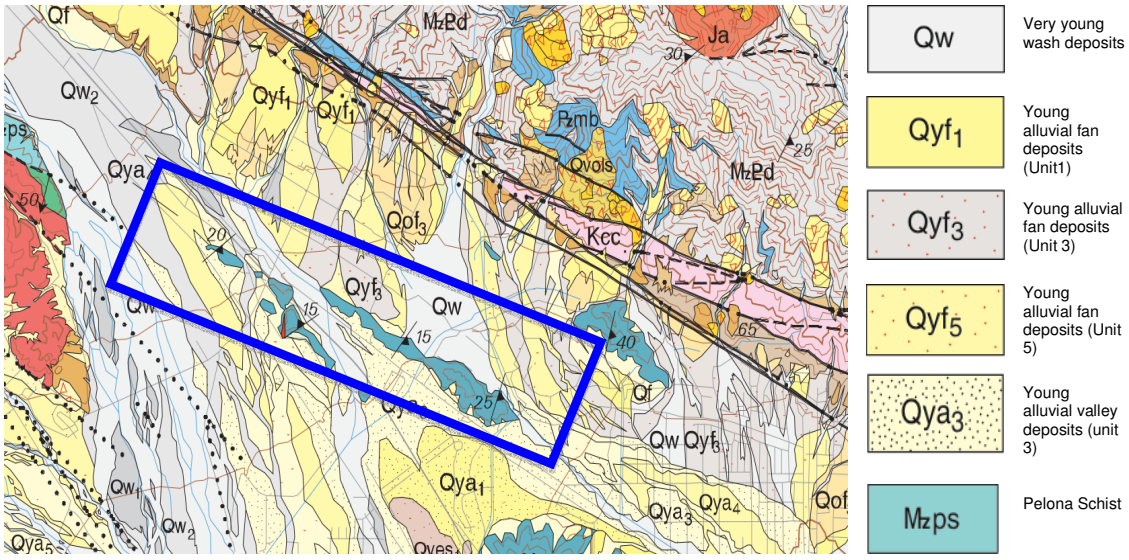

Figure 11. Geologic Map of the San Bernardino Quadrangle where the blue polygon encompassess units in the study area (Morton and Miller, 2006).

Local Faults

The San Andreas Fault, San Jacinto Fault and Mill Creek Fault zones are important geologic features to the project area, and to California (Figure 12). An investigation of these faulting systems was conducted to understand the significance attributed to their presence, and highlight their history. The following is an introduction to studies that have identified several qualities of these three faults.

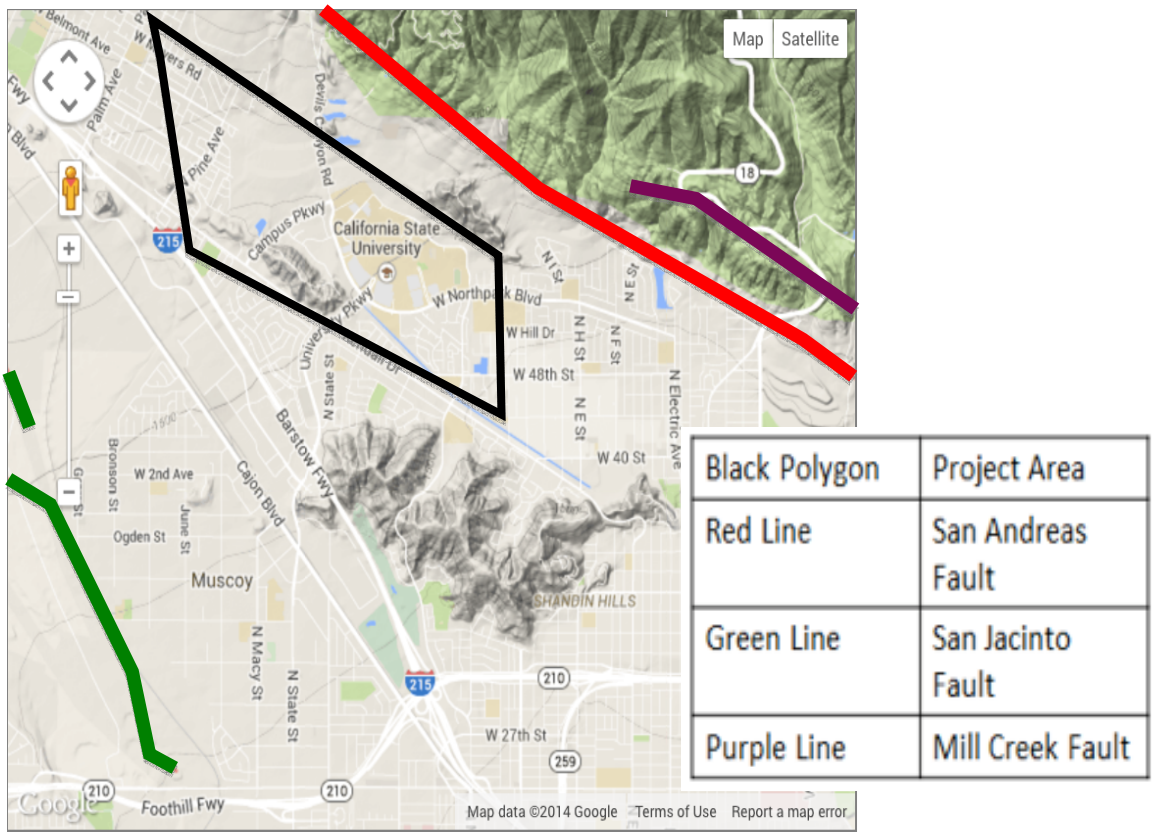

Figure 12. Overview map depicting faults in project area fault. Black polygon, project area, red line, San Andreas Fault, green line, San Jacinto Fault, purple line, Mill Creek Fault (Adapted from Jennings, 1994). Accessed Nov. 5, 2014.

San Andreas Fault Zone

A fault on the Earth's surface is attributed to tectonic activities. These activities are physically apparent in the form of a fault scarp, or unapparent, where offset is hidden beneath the surface. A fault scarp is the displacement of earth where a noticeable physical discontinuity can be identified. The Pacific Plate moves in the northwest direction while the continental plate of North America moves in the southeast direction forming a continental transform fault (Chester, 1993). These movements are attributed to tectonic activities and the San Andreas Fault is a product of these extreme interactions (Mount, 1987). Based upon the stresses and motions the fault has incurred, the fault is classified as a right-lateral strike-slip fault (Stein et al., 1992). The strike of the fault is a term that describes orientation, and is parallel to the actual fault scarp. Segments on either side of the fault, known as blocks, move laterally aside each other, and in some segments, are separated by hundreds of miles (Zoback et al., 1987). For example, areas along the fault between the Tejon Pass and Salton Sea regions have similar geologic features but have been displaced by 150 miles (Schulz and Wallace, 2013). By analyzing the displacement of these segments using such geologic features as alluvial fan deposits and soil age estimates, scientists can extrapolate information regarding slip rates, in addition to identifying particular events that caused the initial rupture.

San Andreas Fault: San Bernardino Mountains Segment

The San Bernardino Mountains segment of the southern San Andreas Fault is located between the Cajon Pass and the San Gorgonio Pass with regions of varying splays (Figure 13). This section of the San Andreas Fault is of primary concern in the project area. The last major earthquake to occur along the segment was in 1812. Since that time, stress upon the fault has continued to accumulate (Freed and Lin, 2002). Historic data suggests major earthquakes along the southern stretch of the fault have been calculated to have variable repeat times of 130 years (Freed and Lin 2002). Based upon this estimate, the San Bernardino Mountains section of the San Andreas Fault is, statistically speaking, 72 years past due for an earthquake event. Due to the fact the last major rupture along the northern interval of the San Andreas Fault was in 1906, southern segments have an increased potential for producing a higher magnitude event (Petersen and Wesnousky, 1994). Estimated plate movement along the entire San Andreas Fault is estimated to be 1.3 inches per year (Jones, 1995).

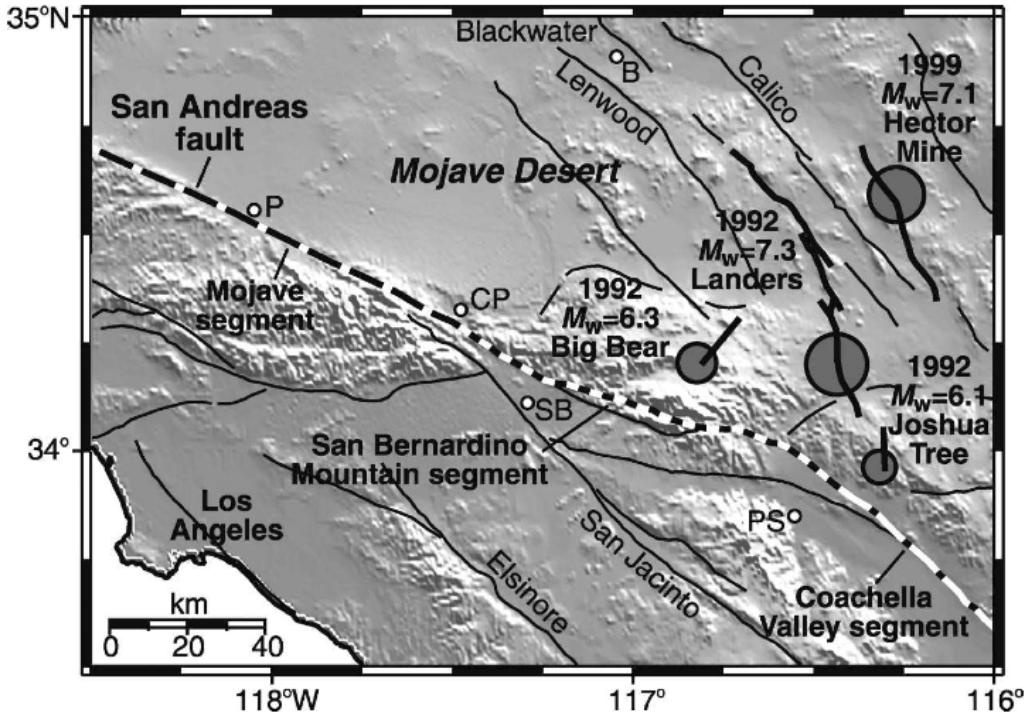

Figure 13. A map depicting several segments of the southern San Andreas Fault interval. This study addresses the San Bernardino Mountains segment, located between Cajon Pass and San Gorgonio Pass (Freed and Lin, 2002).

Considering the complexities of the San Andreas Fault, it is difficult to sum up its nature. This is apparent in regards to its vast length, varying characteristics from one segment to another, history, and ability to produce earthquakes. Moreover, by studying these intricacies and relating them to one another, one can began to identify the attributes that the fault contains. This structuring, allows for an intelligent interpretation and assumption as to how the fault may behave. Although this method of analysis is not 100% accurate, it does give the best possible model to understand past, present and future events.

San Jacinto Fault

In the project area, the San Jacinto Fault is located southeast from the San Bernardino Mountains segment of the San Andreas Fault as shown in Figure 12. It is classified as a right lateral strike slip fault, with zones of northeast trending left lateral fault splays, and extends for 210 kilometers (Petersen and Wesnousky, 1994). The fault has produced the highest rate of moderate to large earthquakes compared to all other faulting regions in southern California according to Petersen and Wesnousky (1994). The last significant rupture of the San Jacinto Fault occurred on April 9th, 1968 along the Coyote Creek segment of the fault, producing a magnitude 6.5 earthquake. Depending on the segment along the San Jacinto Fault zone past studies suggest a rupture interval ranging from 100 to 300 years (Wesnousky, 1986). Fault slip rates have been estimated by observing and measuring alluvial fan and stream channel offsets, and have been found to range from 7 to 17 millimeters per year. Jones (1995) predicted the probability of a future earthquake ranging from 6.5 to 7.5 in magnitude.

Mill Creek Fault

Of the above faults zones, the Mill Creek Fault has the least amount of information available. Located just northeast from the San Bernardino Mountains segment of the San Andreas Fault, it stretches for approximately 80 km, with one end of the fault originating close to the southeastern edge of the San Bernardino Mountains segment of the southern San Andreas Fault. These observations are

based upon Figure 12 and a fault activity map of California produced by Jones (1995). In addition, Jennings (1994) provides an estimated relative age for the last major rupture of the fault to have occurred in the Late Quaternary period. This estimate is based upon the displacement of sediment layering of the same time period.

Areas of Interest

This study focuses on a refraction microtremor analysis (ReMi) along several roads around the California State University San Bernardino area (Figure 12). Shear wave velocity data was collected at 30 locations. The San Andreas Fault is close to the campus and surrounding residential areas, with the furthest point of data collection being less than 2 miles away from the fault trace. The closest area of data collection to the San Andreas Fault was within 0.25 miles. The aptness for each area of study was dependent on the proximity to the San Andreas Fault, and also on the variety of geologic units. Obtaining multiple shear wave velocity profiles in diverse geologic units provides an indication of potential ground motion in corresponding subsurface material. Several experimental areas were chosen based upon their proximity to housing developments, schools and local businesses.

CHAPTER FOUR

EXPERIMENTAL DESIGN

Project Set-up

As previously stated, 30 shear wave velocity profiles were acquired in areas surrounding communities of California State University San Bernardino. Array spreads contained 24 geophones (3m separation), with a standard array length of 69 m. Exceptions were array lengths of 57.5 m and 96 m (two each). The locations of these exceptions are highlighted in the results. Each array is linear, where the standard length is a span that could be effectively deployed within several field sites when considering space limitations and depths of investigation. The two profiles that had a length of 57.5 m, with a geophone spacing of 2.5 m, were limited spatially within areas of investigation. The two array profiles 96 m in length had a geophone interval of 4 m, and were not constrained by spatial limitations, allowing for an expanded investigation.

When preparing array spreads in the field, several pieces of equipment are necessary, which are listed below. Before deploying any field equipment, an appropriate area of study must be identified. Many factors go into identifying an ideal location. Such factors include: close proximity to a continuous seismic source, having an even surface devoid of elevation changes, avoidance of artificial (man-made) surface compositions, and being spatially adequate to accommodate profile spread lengths of at least 57.5 m. Once these criteria are

met in an area of study, the deployment of field instruments begins with the measurement of the length of a profile array. Using the measuring tape as a guide to ensure a linear array is constructed; geophones (Figure 14) are inserted according to a specific interval. It is imperative that arrays are as straight as possible. In the case of this experiment, the majority of the profiles had a geophone spacing of 3 m, with a spread length of 69 m. It is essential that the staked geophones be properly coupled to the ground while maintaining an orientation, which is normal to the earth's surface. In areas where the ground is hard, a metal stake and hammer are used to facilitate geophone placement by hammering the stake into the ground to produce a hole in which the geophone can be placed. Once all 24 geophones are in place, they are connected to receiver cables in a 6-12-6 orientation. Each receiver cable has 12 connection inputs (Figure 15). For the first 6 geophones of the spread, 6 are connected to the first receiver cable. The next 12 geophones connect to the second receiver cable. The final 6 geophones are connected to the third receiver cable. After all geophones are connected, receiver cable output plugs are connected to two Seistronix EX-12 data loggers (Figure 16). One Seistronix battery pack, Figure 17, is connected to each data logger. The last step of the assembly is to connect either end of the spread to a computer interface. Figure 18 depicts a deployed profile array in the field. This process is completed within 15 minutes using a two-person team. The following list of equipment, for array construction, utilized in the field as follows:

1) Computer interface running EX-6 System Software

2) Data logger: Seistronix EX-12 (2)

3) Data logger batteries: Seistronix BP-1 Battery Pack (2)

4) Receiver Cables (3)

5) 10 Hz vertical geophone receivers (24)

6) 100 m measuring tape

7) Metal stake and hammer

8) GPS Device

Figure 14. Depicted above are the 10 Hz vertical geophones used in the study area. They have a two pronged output connection to couple with receiver cables.

Figure 15. Receiver line cable with two input connections. Geophones have two prongs that connect to two terminals along one input connection.

Figure 16. The Seistronix EX-12 data logger used to connect the 24 geophones. Receiver cables are connected at either end of the data logger.

Figure 17. The BP-1 battery pack, which connects to the data loggers.

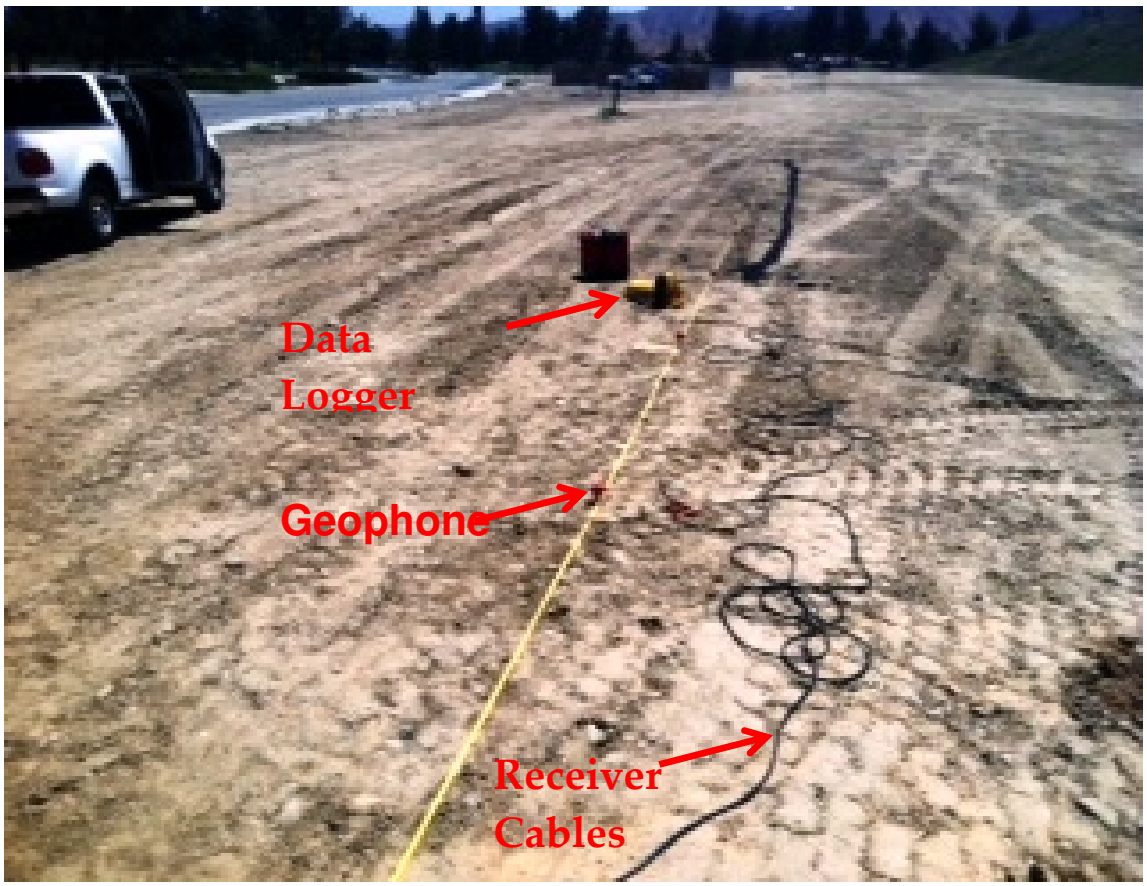

Figure 18. Depicted here is an in situ profile array deployed in the field. Shown above are the orientation of geophones, receiver cables, and data logger.

Experiment Area Identification

The project area was selected based upon several factors. These included: areas of recent land development for housing and businesses, proximity to continuous seismic sources, observed geologic units and proximity to the San Andreas Fault. Using these factors, the study area was divided into three zones of investigation (Figure 19). Each zone represents an expansion of

the study area, which began in areas surrounding California State University San Bernardino, Zone 1. As Figure 20 depicts, subsequent zones were expanded to the northwest, where geologic units became more diverse and proximity to the San Andreas Fault increased. This is important to the overall success of the study because subsequent data gathered in differing geologic units were more representative of the subsurface characteristics in the project area as a whole.

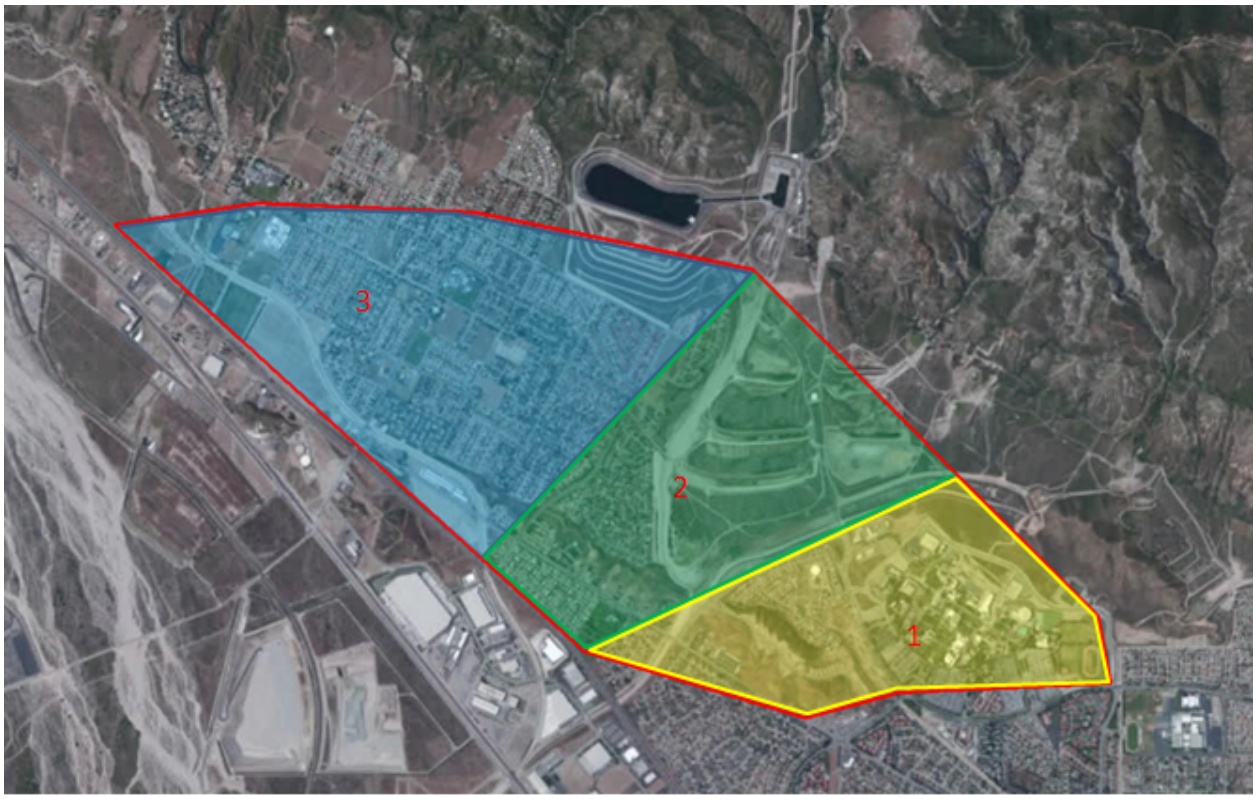

Figure 19. Three zones of investigation. Each zone corresponds to a progression of the experiment, where Zone 1 encompasses areas surrounding California State University San Bernardino.

Data Collection

Once the profile array is assembled, data acquisition specifications must be made within the boundaries of the Seistronix software. These specifications include selecting the sampling interval and defining data acquisition settings to continuous mode. These parameters determine how long one record will record continuously. All records in this experiment have a recording duration of 32 seconds. Once these settings are in place, the next step is to check the functionality of the geophone spread. This is done by testing the resistance for each of the 24 geophones to ensure data are recorded properly (Figure 20). In the case where geophone resistance is lower than the specified threshold, the geophone is either not connected properly to the receiver cables, is poorly coupled with the ground in which it is staked, or there is a malfunction in equipment. There are two ways in which a geophone can be improperly connected to the receiver cables. The first being that the receiver clamps are not in proper contact with the receiver cable terminals, or the geophone is connected in an incorrect location along the receiver cable line. Staking in an environment where sediment is extremely soft or loosely consolidated, or where the ground is extremely hard and impenetrable can cause poor coupling of geophones. The use of a stake and hammer to facilitate geophone insertion almost always eliminates the latter problem. After quality control inspection of the array line, data acquisition is set to begin. If acquisition is taking place in close proximity to

a busy street or freeway with constant traffic, the software is manually triggered to record wave arrivals.

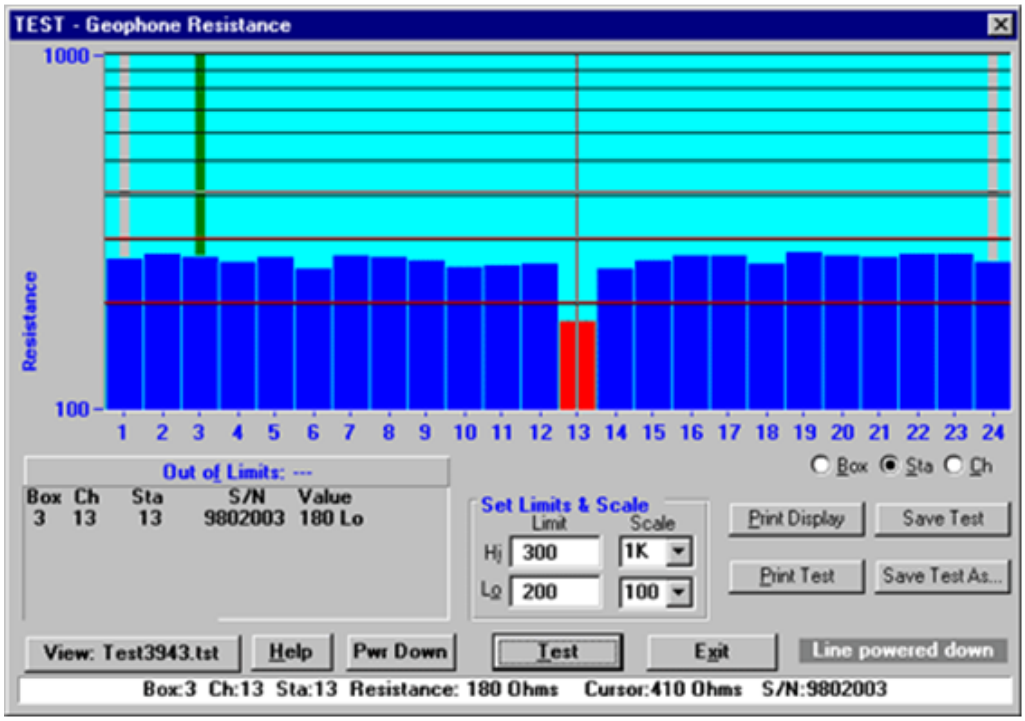

Geophone Resistance Test

Figure 20. A screen shot from Seistronix EX-12 software where geophone resistance is tested. The 13th geophone is shown having low resistance and should be checked to ensure it is coupled and functioning properly.

As stated, the recording interval for one record is 32 seconds. Once a record is complete, the data is saved in a (.dat) file format. Data acquisition for the next record commences immediately, repeating the process as outlined for as many records that need to be recorded (12-13 in the case of this experiment). In areas where traffic is not flowing heavily and cars approach the profile array in discontinuous clusters, a pause between recording data is an

effective way of utilizing semi-continuous seismic sources. A standard and valuable quality control method is to observe the field seismogram generated to make sure data acquired is visually acceptable.

CHAPTER FIVE

DATA PROCESSING

Field Record Conversion

As explained in Chapter 3, after obtaining field records in a time-spatial domain, the field data are processed to transform records to a slowness-frequency domain (p-f). Using SeisOpt Vspect data processing software, seismic records are converted from SEG-2 to SEG-Y file types (Figure 21). This conversion allows the software to read and analyze the data. After conversion, records, are imported as a group, where one group represents data acquired from one profile, and checked to ensure appropriate data specifications are applied (Figure 22). One field experiment is representative of a set of records, where a set of records contains 24 seismograms for 24 geophones, and a plane is a recording for one experiment. For a given location, 12 to 13 experiments were conducted.

Once the data files are imported and specified, an image is generated depicting recording time and trace amplitude for each plane within one group (Optim, 2006). These attributes are crosschecked to ensure the recording time and number of seismograms are correct. The software enables scrolling of all planes within one group for quality control (Figure 23). Once records are crosschecked, plot parameters are identified (Figure 24). The plot parameters consist of elements per vector, vectors per plane, and number of planes (Optim,

2006). Elements per vector are defined as the total recording time divided by the sampling interval. For example, the standard recording time for seismic records acquired in the field is 32 seconds with a sampling interval of 2.0 msec. Thus, the overall elements per vector are 16000. The number of channels per plane is equal to the number of geophones used to record seismic wave arrivals in the field, i.e. 24. The number of planes represents the number of separate experiments being analyzed, in this case 12-13.

After specifying plot parameters, equalization of traces is performed using the pre-processing tool (Figure 25). This procedure normalizes the data and prevents high amplitude outliers from skewing resultant p-f spectrums (Optim, 2006). Once complete, trace header geometry is erased and manually specified by inputting the number of records to be analyzed, along with the amount of channels/geophones used and spacing (Figure 26). In this experiment, 12-13 records were gathered for every one profile in the field, where each record utilized 24 geophone receivers, most with 3 m spacing. By indicating the geometry of the records being read, the software identifies the spatial orientation in which the seismic data was collected. Following the specification of space header geometry, parameters for the p-f spectrum are classified (Figure 27). Sampling intervals (0.002 msec), geophone spacing (3m), maximum frequency for p-f transformation (35 Hz), predicted minimum velocity (100 m/s), and direction of seismic wave acquisition along geophone arrays (both directions) are all defined prior to spectrum construction (Optim, 2006). Maximum frequency

and predicted minimum velocities are manually fine-tuned based upon the interpreted quality of the p-f spectrum produced. Figure 28 depicts the generated p-f spectrum. A p-f spectrum is generated for each plane/record uploaded for analysis. This is important because in succeeding steps, several records are combined/stacked to generate one smooth p-f spectrum image, which is the basis for shear wave velocity analyses. Based upon the quality of the images, and ability to identify prominent dispersion amplitudes, records are modified, discarded or retained. The ability to remove records that produce low quality p-f spectrums ensures that when subsequent records are stacked, the resulting image is optimal, excluding undesirable data processing artifacts and outliers (Figure 29).

Once records are examined/filtered for quality control, and stacked, a final p-f velocity spectrum is constructed. Along the dispersion curve, which trends from the top left corner to the lower right of the spectrum image, several “picks” are made (Figure 30). The process of “picking” entails choosing several points along the dispersion amplitude curve representing slowness-frequency pairs by (Optim, 2006). This is made possible by interacting with the spectral image by “right-clicking” with a mouse in areas of interest. Several points are chosen from the top left corner of the curve down to the right in areas with high spectral ratios. Following these constraints, picks accurately represent real velocity values (Optim, 2006). These areas with high spectral ratios are represented as transitions from the color blue to green along the trend of the dispersion curve.

This process continues until the curve is no longer distinguishable. Picks are then saved as a text file (Figure 31) and uploaded within the ReMi Disper software, where they are inverted to produce a velocity model (Figure 32).

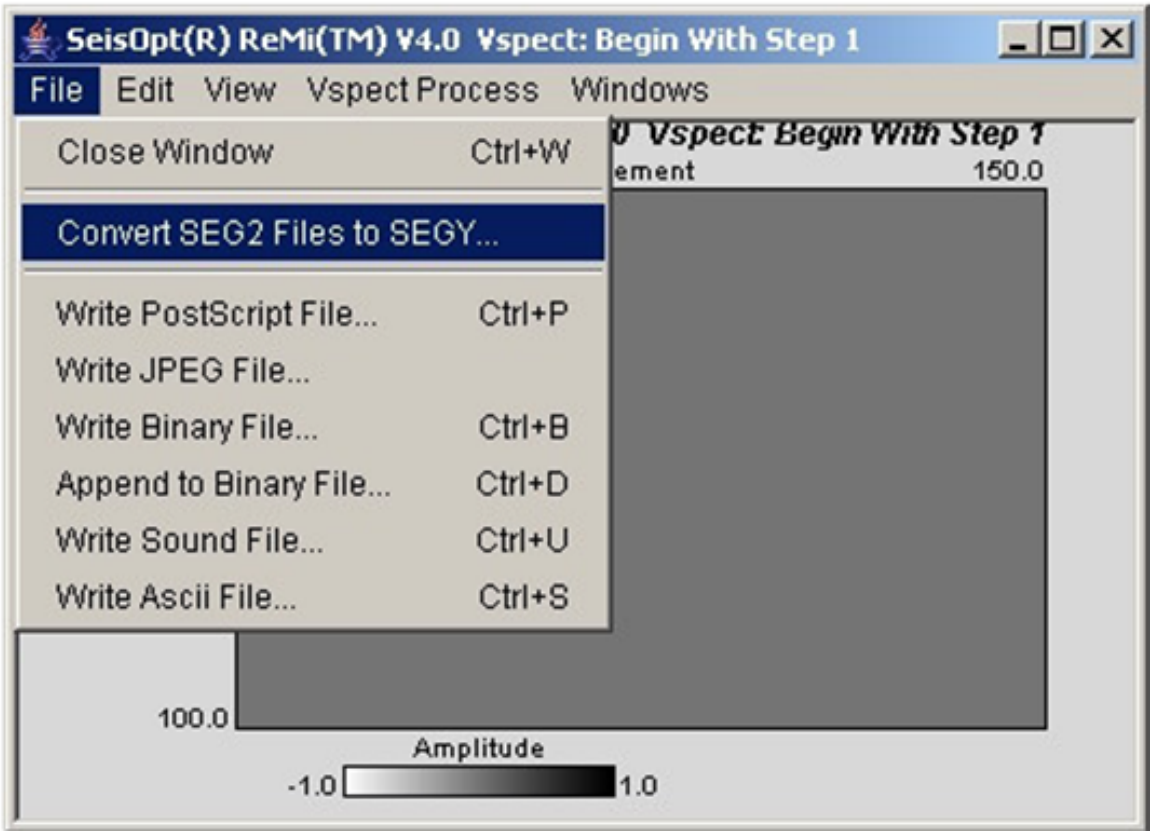

Figure 21. Seismic records gathered in the field with a .dat file extension are SEG-2 files and are converted to SEG-Y format, to allow processing within the, Vspect software. Each profile may contain 12-13 records that need to be converted.

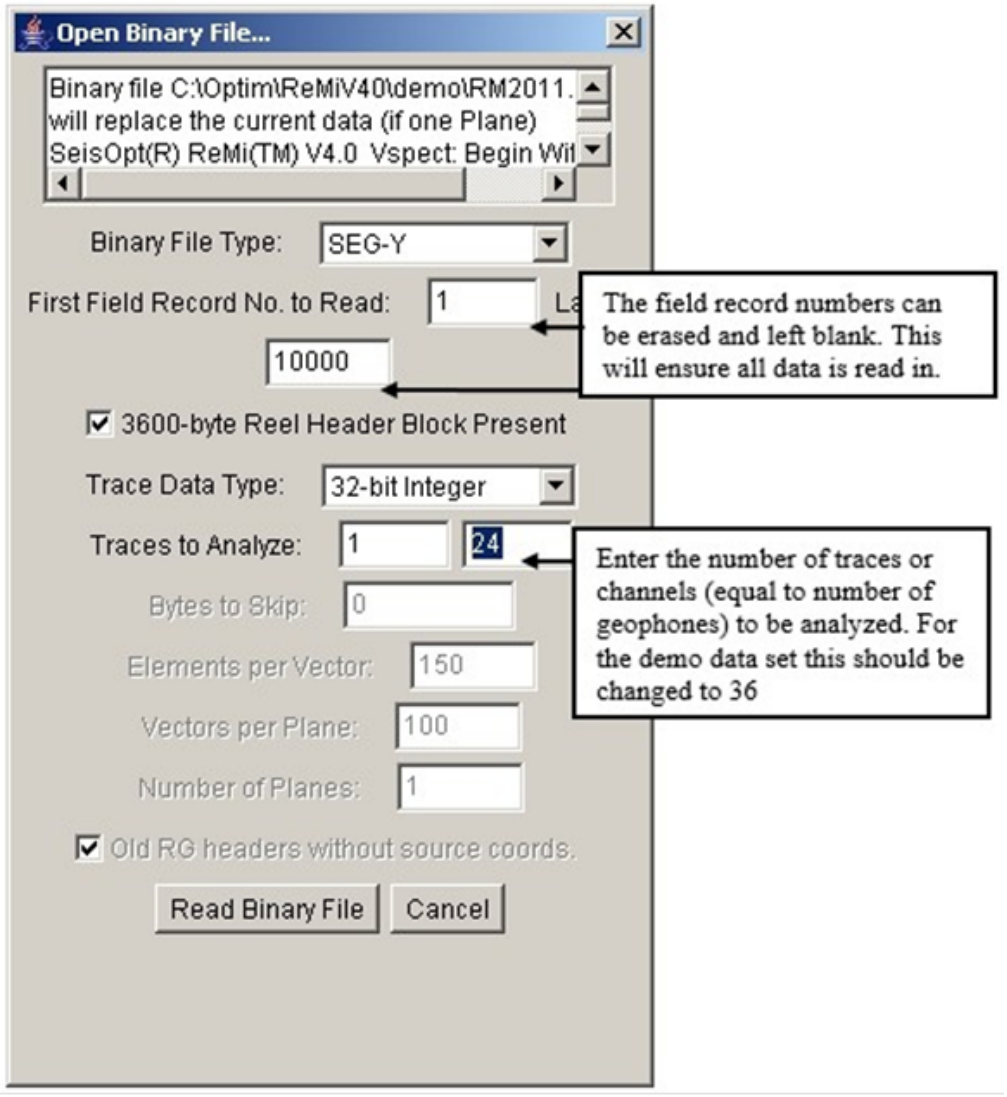

Figure 22. When opening converted data records, specifications are input. The "First field Record No. to be read" category is left blank, the "Trace Data Type" is 32-bit integer, "Traces (geophones) to Analyze" is 24, and all other catergories are left unchanged (Optim, 2006).

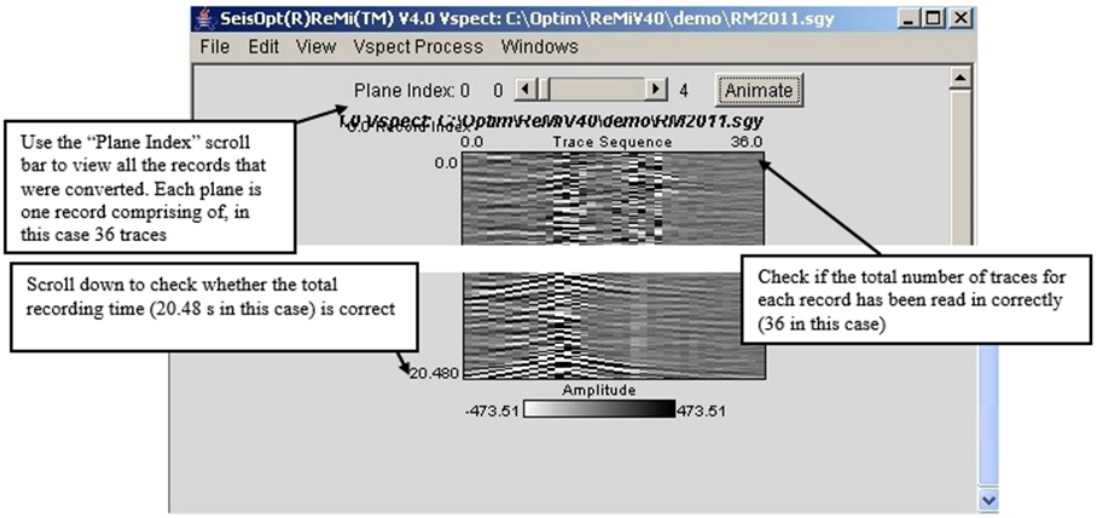

Figure 23. After loading records and inputting data specifications, loaded records are inspected by scrolling through the "Plane Index" to ensure that: all records that are going to be read are present, the total number of traces is correct (trace sequence), and the total recording time is accurate (record index). The x-axis is the trace sequence, and y-axis, the record index (Optim, 2006).

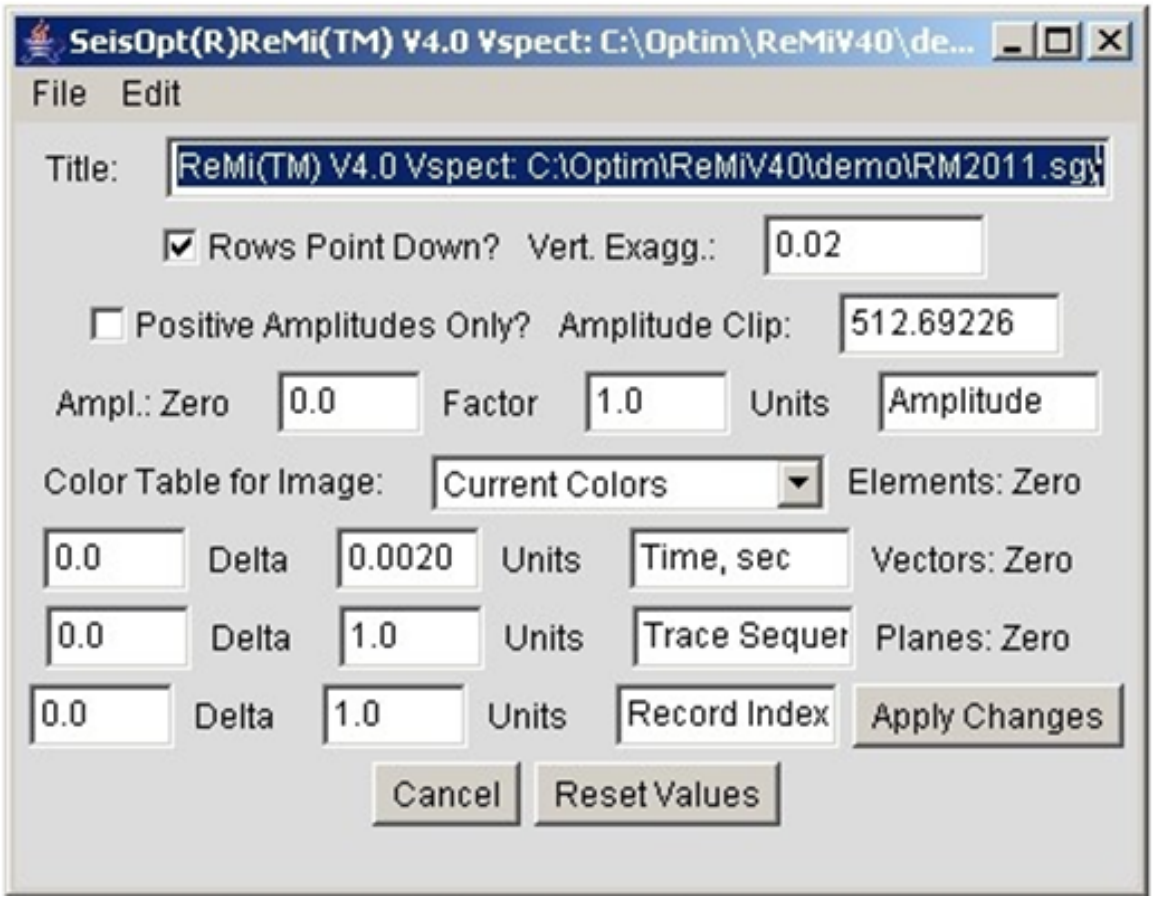

Figure 24. Specification of plot parameters allows for records to be analyzed more effectively. By checking the box “Rows Pointing Down”, the axis for time is orientated in a descending fashion. “Vertical Exaggeration” defines the overall scale of the plotting area (Optim, 2006). Specifying the “Amplitude Clip” value ensures that all values above the input are disregarded during data analysis. “Elements: Zero” represents the starting time for each record. For this experiment, starting time is zero. A sampling rate of .002 seconds is inputted into the “Elements Delta”, where element units are in seconds (Optim, 2006). “Vectors: Zero” indicates the starting distance for each record, which is zero. “Vectors Delta” designates geophone spacing, where vector units are in meters. “Planes: Zero” represents the beginning of the plane/planes that are being analyzed. For this experiment it begins with the 1st record of a batch. “Planes Delta” defines how planes are labeled after the first (Optim, 2006).

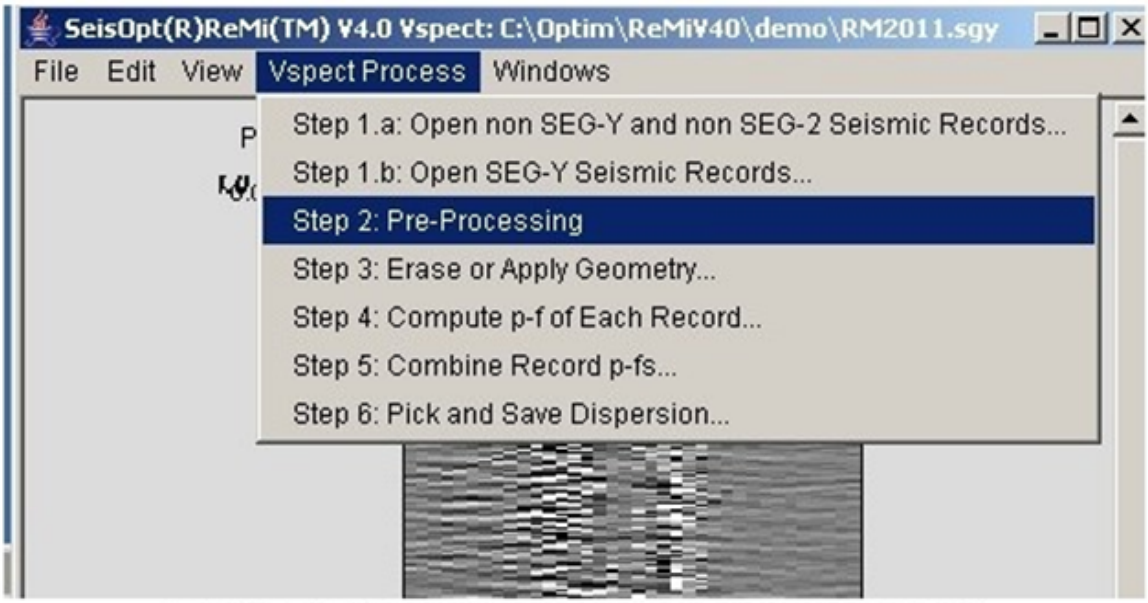

Figure 25. The “Pre-Processing” feature normalizes the traces by performing gain control equalizations (Optim, 2006). This tool reduces data outliers and aberrations to give an accurate and robust p-f spectrum superior to one created without normalization (Optim, 2006).

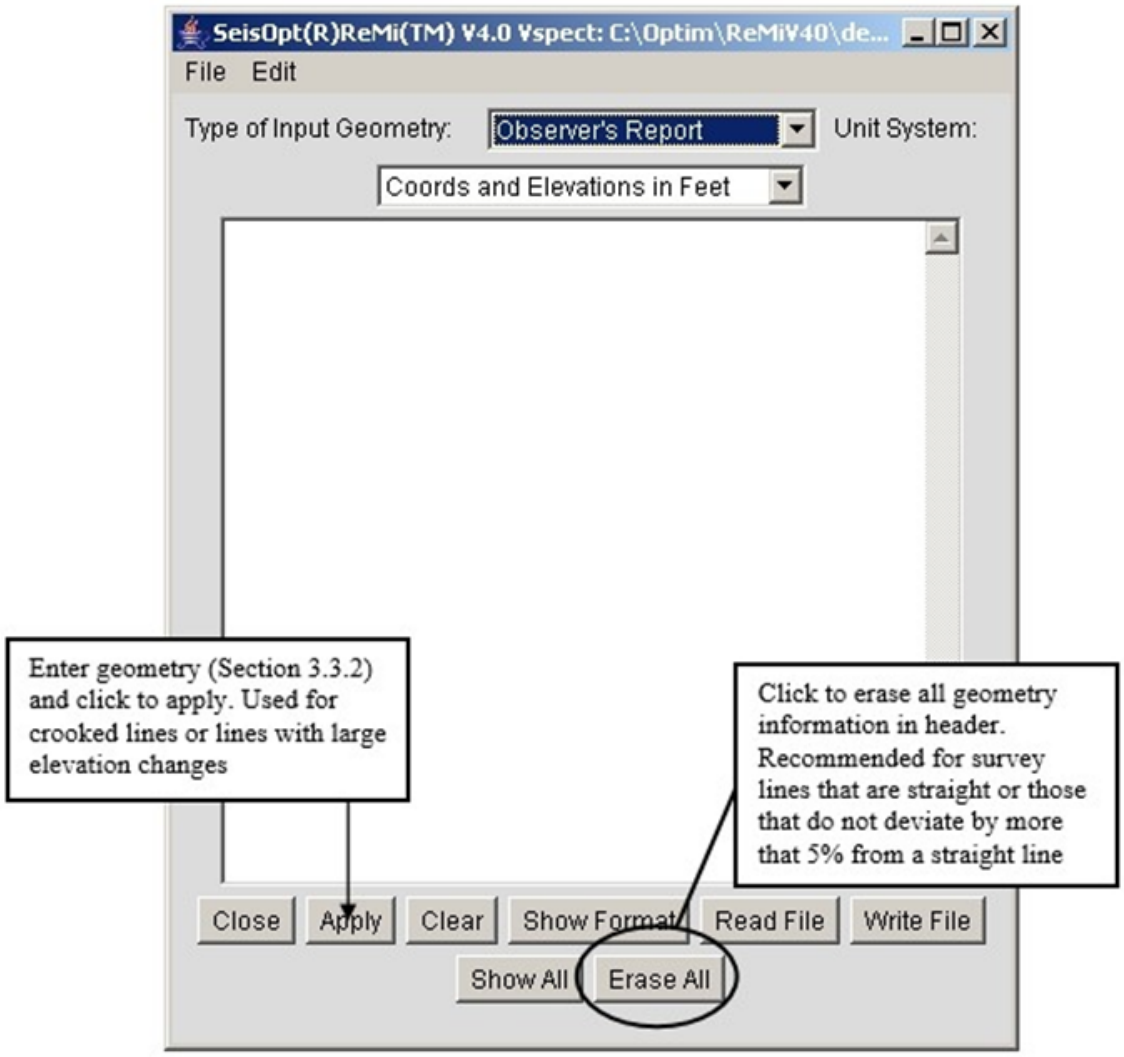

Figure 26. Erasing default geometry and manually inputting the geometry of the geophone array orientation ensures the p-f spectrum output is accurate. The number of channels/geophones and geophone spacing are inserted in the above window. The unit system should be in meters (Optim, 2006).

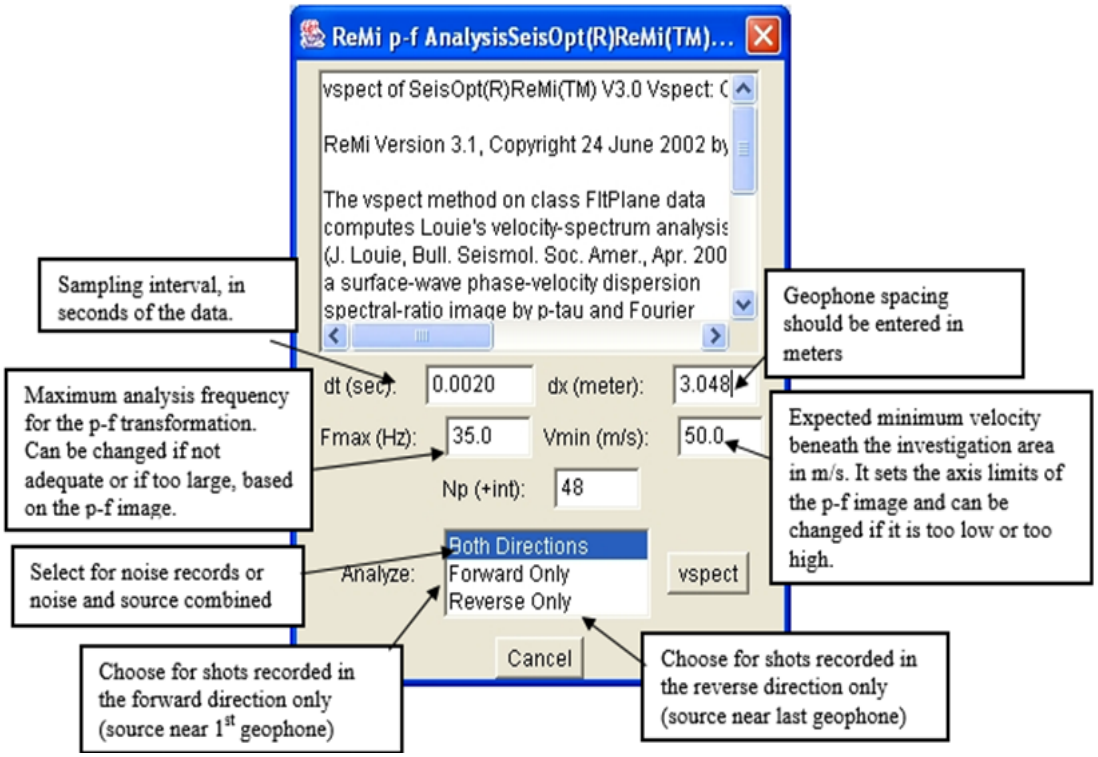

Figure 27. Depicted is the p-f spectrum specification window. A sampling interval of 2 msec is input in the dt (sec) category. Geophone spacing for the group (typically, 3m, but 2.5 and 4m for several) is input in the "dx (meter)" category (Optim, 2006). The maximum frequency to be analyzed is "Fmax (Hz)". The value input can vary above or below 30 Hz depending on the clarity of the p-f spectral image. This value can be changed until a suitable frequency is identified (Optim, 2006). The "Vmin (m/s)" category signifies the minimum estimated velocity of the subsurface. This, like the "Fmax" can be modified until the p-f spectral image is visibly suitable. The value input here can be above or below a baseline minimum velocity of 100 m/s. The value entered in the "Np (+int)" category represents the amount of slowness in the analysis. A software default of 48 s/m is appropriate (Optim, 2006). Because the ReMi method obtains wave arrivals from several directions, the "Analyze" category is set in both directions (Optim, 2006).

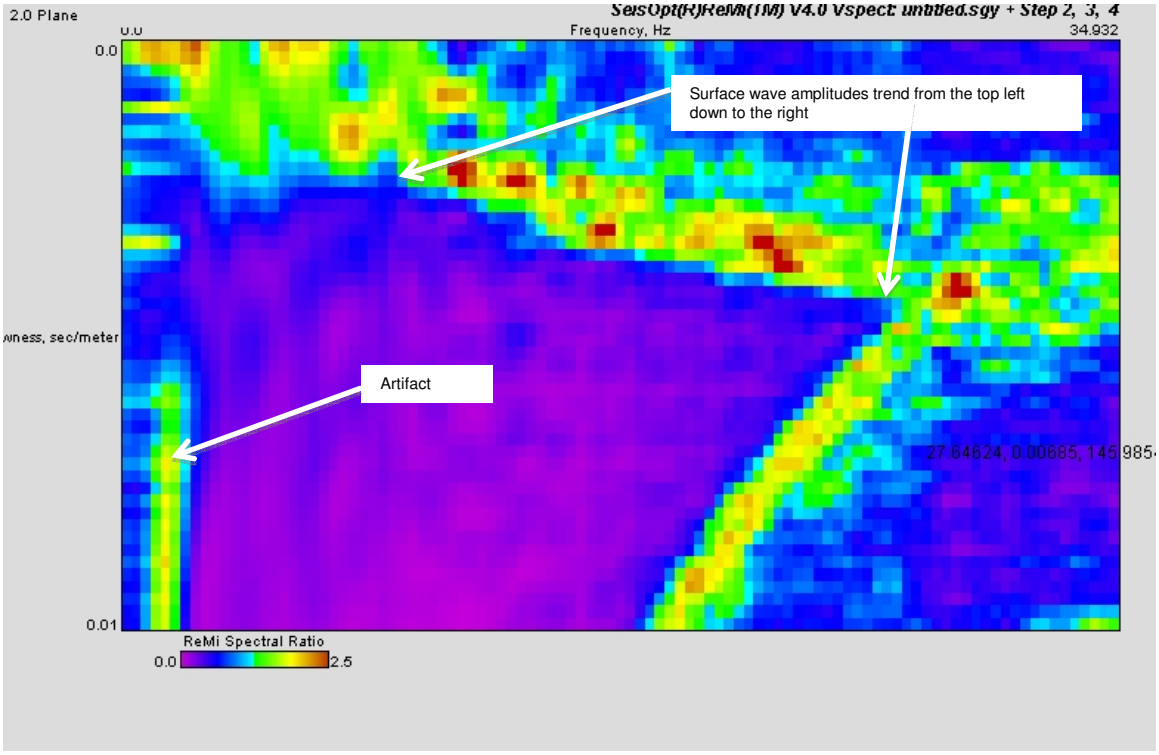

Figure 28. Here is an example of a p-f spectrum where the y-axis represents slowness in sec/meter and the x-axis represents frequency in Hz (Optim, 2006). Dispersion amplitude from wave arrivals is identified as a curve that begins in the upper left corner of the image and trends down to the lower right. Other features are present within the spectrum but are not relevant to the trend of the curve of interest.

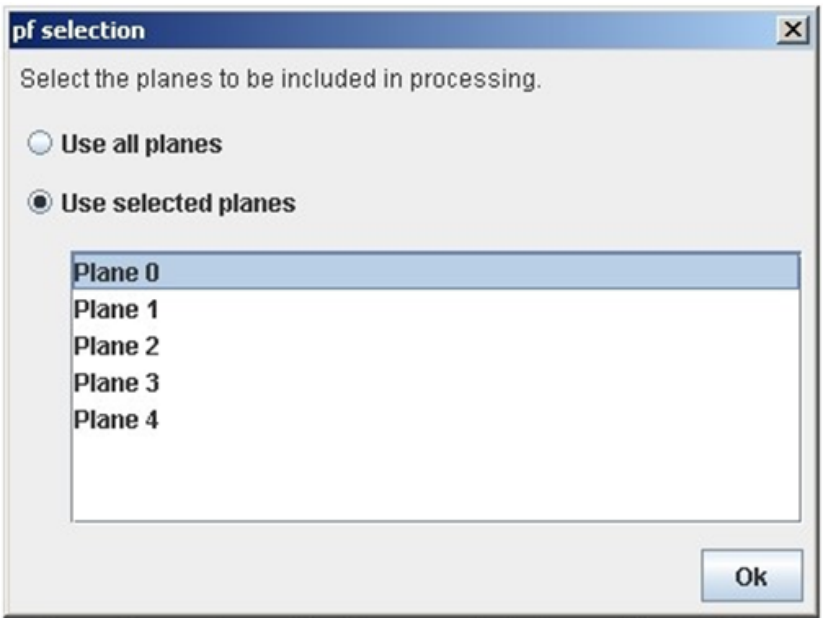

Figure 29. After scrolling through multiple planes/records and examining each p-f spectrum, depending whether or not the spectrum is of high quality, they are either kept or discarded. Spectra of high quality, demonstrate a clear dispersion amplitude curve trending from the top left to the lower right. If a spectrum cannot be resolved by adjusting the maximum frequency to be analyzed and/or the minimum velocity expected in the p-f spectrum specification window, it is removed from the group. If all, or the remaining planes are adequate, they are stacked to generate one p-f spectrum image.

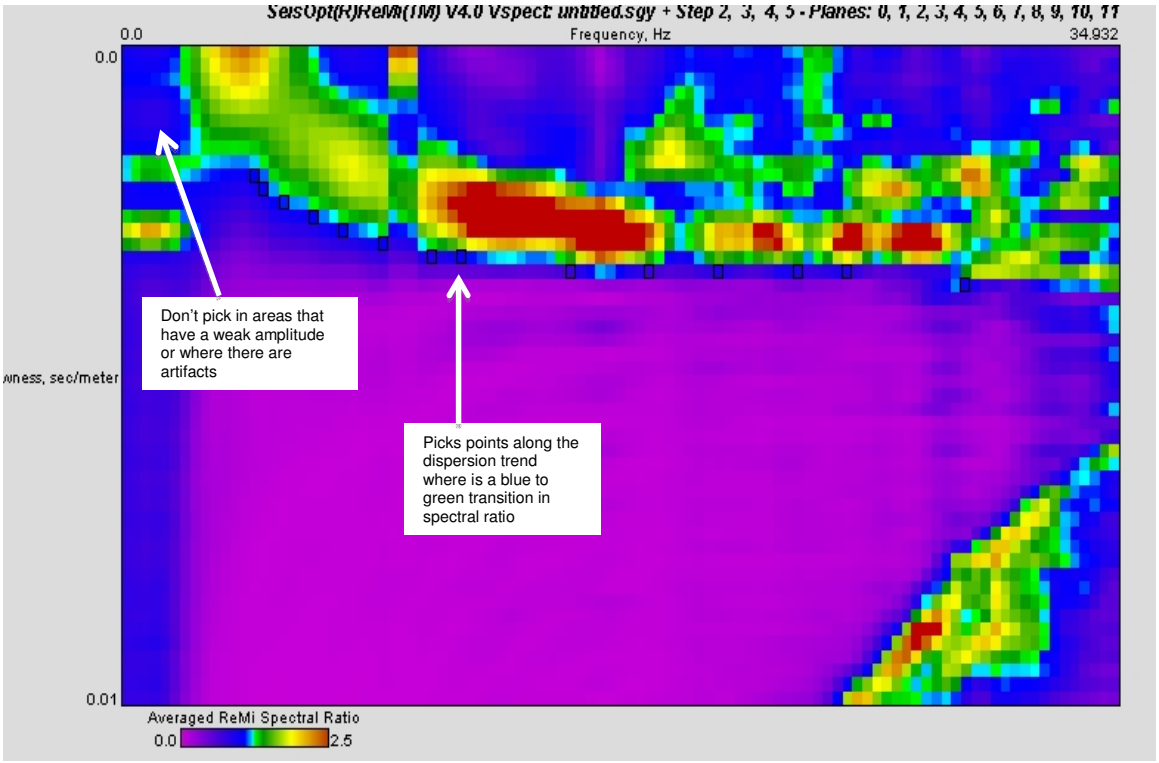

Figure 30. Once desired planes are filtered based upon the quality of p-f spectra, they are stacked to produce a p-f spectrum image which represents all desirable data from a profile array. Using this image, the process of picking the dispersion curve is comences. These picks are represented by the black boxes along areas of low spectral ratio (blue) and strong amplitude. The picks represent slowness/frequency coordinates. The color scheme of the image can be adjusted to facilitate this process. Picking should not be conducted in areas where the dispersion amplitude is weak or where artifacts are present.

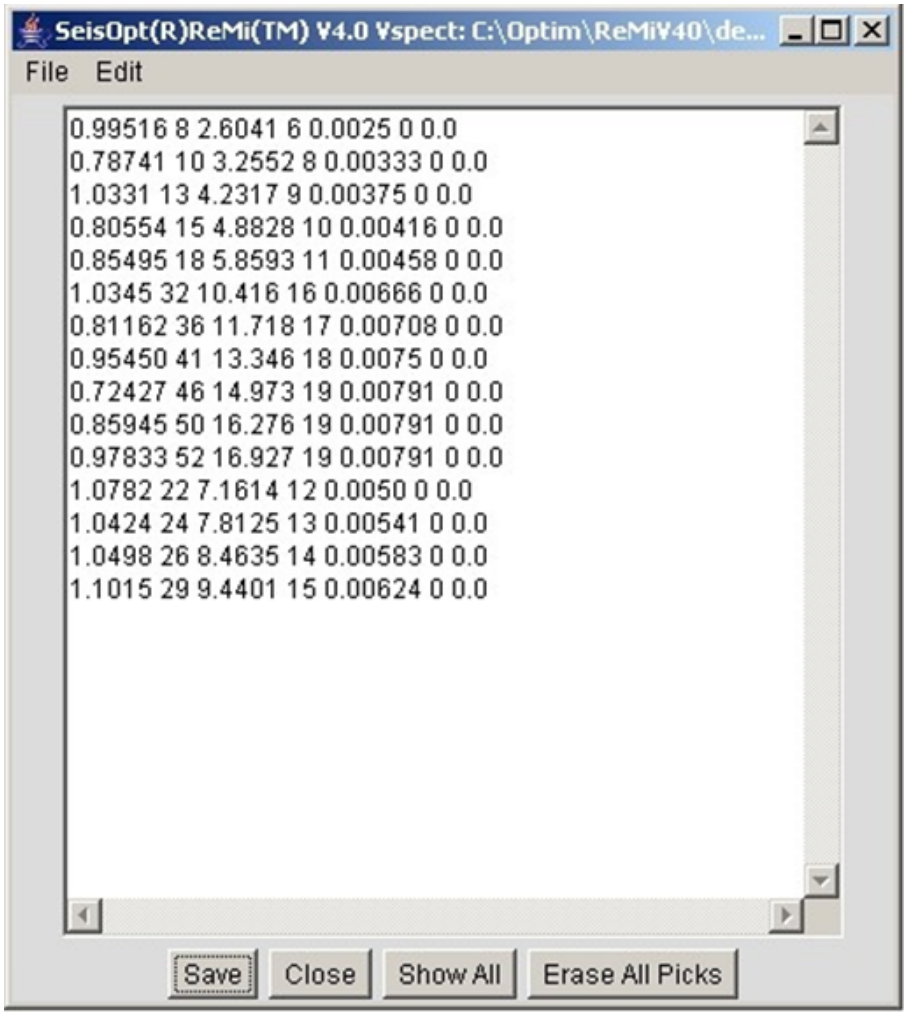

Figure 31. After picking along the curve, the values are saved and uploaded to the ReMi Disper software for further processing.

Velocity Model Construction

Once picks are uploaded into ReMi Disper software, a stratigraphic model depicting depth, density, layer thickness and layer velocity is constructed via the software. In addition, a dispersion curve showing velocity (v) vs. period (T) is fit to the pick points selected along the dispersion curve of the p-f histogram (Figure 33). The dispersion curve is an inversion of slowness vs. frequency data with values being in the velocity vs. period domain. An RMS (root mean squared) error, along with site classification is also produced. By modifying the number of layers and thickness of the default stratigraphic model, the velocity-period curve forms a better fit to the points. Input parameters for the depth of investigation are set at 50 m. This was done to ensure that there were not any abrupt changes in velocity at depth, but subsequent shear velocity calculations and site classification determination only takes into account the first 30 m within the subsurface. Density is held constant and remains unchanged. This process also affects the RMS and calculates site classification. The goal is to get the best fit of the dispersion curve to the pick points, produce a stratigraphic model, and reduce the RMS error as low as possible while still maintaining a realistic model. An automatic algorithmic feature within the software can be used to provide these modifications, but even when using this feature, manual changes must be made to attain the best model.

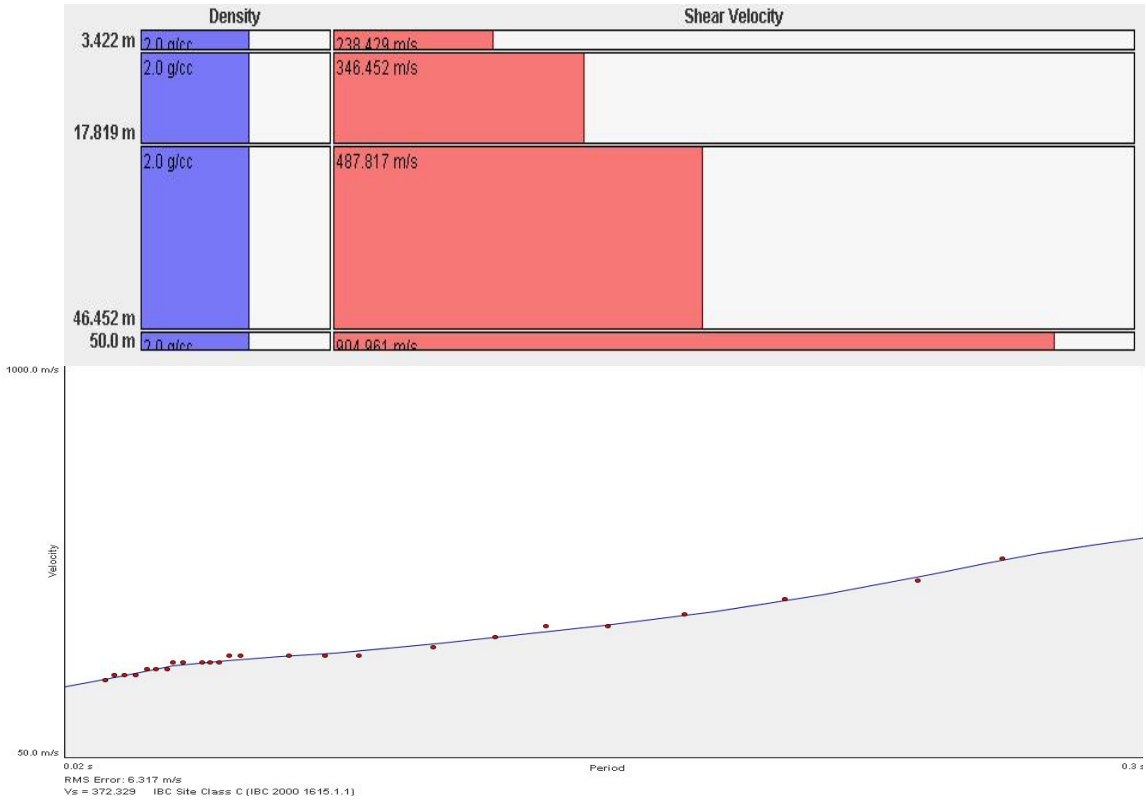

Figure 32. This figure depicts the ReMi Disper software with picks uploaded from ReMi Vspect. A stratigraphic velocity model is present in blue and red in the middle of the figure and a dispersion curve is at the bottom of the figure. The stratigraphic velocity model has four characteristics: thickness, density, number of layers and velocity. The thickness and amount of layers can be modified to fit the dispersion curve to the picks represented by the red points. These points are the inverse of the picks along the dispersion amplitude of the p-f spectrum. The inversion of slowness and frequency is velocity and period, where velocity is the y-axis and frequency is the x-axis of the dispersion curve. The dispersion curve example above has yet to be fit to the trend of the pick points. The software is capable of automatically fitting the curve to the points. This is useful in reducing the RMS error during the fitting process. Once the pick points fit, final shear wave velocity (Vs) and International Building Code (IBC) site classification values are given. The IBC and NEHRP metric mirror each other.

CHAPTER SIX

RESULTS

Data Collection

The project area is broken up into three zones of investigation. The first zone contains ten profiles, which are located around the California State University San Bernardino campus (Figure 33). The shear-wave velocities and site classifications for each profile within Zone 1 are listed in Table 1. Eight of the ten profiles deployed yielded a site classification of C, where shear wave velocities ranged from 372 m/s to 554 m/s. The two other profiles produced a site classification of D where shear wave velocities range from 321 m/s to 331 m/s. One p-f spectrum, dispersion curve and stratigraphic velocity model were provided as an example of data acquisition within each zone. All data for the remaining profiles is available upon request. Figure 34 depicts the p-f spectrum for the first profile in Zone 1, which resides in the wash deposit (Qw) geologic unit. A dispersion curve for Profile 1 is shown in Figure 35, and in Figure 36 a velocity model is presented, having four stratigraphic layers, each of varying thickness and velocity. The first layer is 3.4 m thick having a velocity of 238.429 m/s, the second layer is 14.3 m thick with a velocity of 346 m/s, the third layer is 28.6 m thick with a velocity of 487 m/s. meters thick and the fourth layer is 3.5 m thick with a velocity of 904 m/s. The Vs30 value for profile 1 was 372 m/s with a site classification of C.

Figure 33. Depicted above is zone 1 with containing 10 profiles.

TABLE 2. ZONE ONE PROFILE DATA

Profile #	Line Length (meters)	Geophone Spacing (meters)	Vs30 (m/s)	Site Classification	Latitude	Longitude
1	69	3	372	C	34°10'47.65"N	117°19'43.07"W
2	69	3	321	D	34°10'49.52"N	117°19'44.62"W
3	69	3	331	D	34°10'51.81"N	117°19'45.98"W
4	69	3	392	C	34°10'54.88"N	117°19'47.50"W
5	69	3	444	C	34°11'5.56"N	117°19'51.60"W
6	92	4	391	C	34°10'41.62"N	117°19'5.53"W
7	92	4	441	C	34°10'44.49"N	117°18'58.86"W
8	69	3	419	C	34°10'57.87"N	117°18'53.45"W
9	69	3	554	C	34°11'11.63"N	117°19'26.99"W
10	69	3	519	C	34°10'41.34"N	117°20'2.85"W

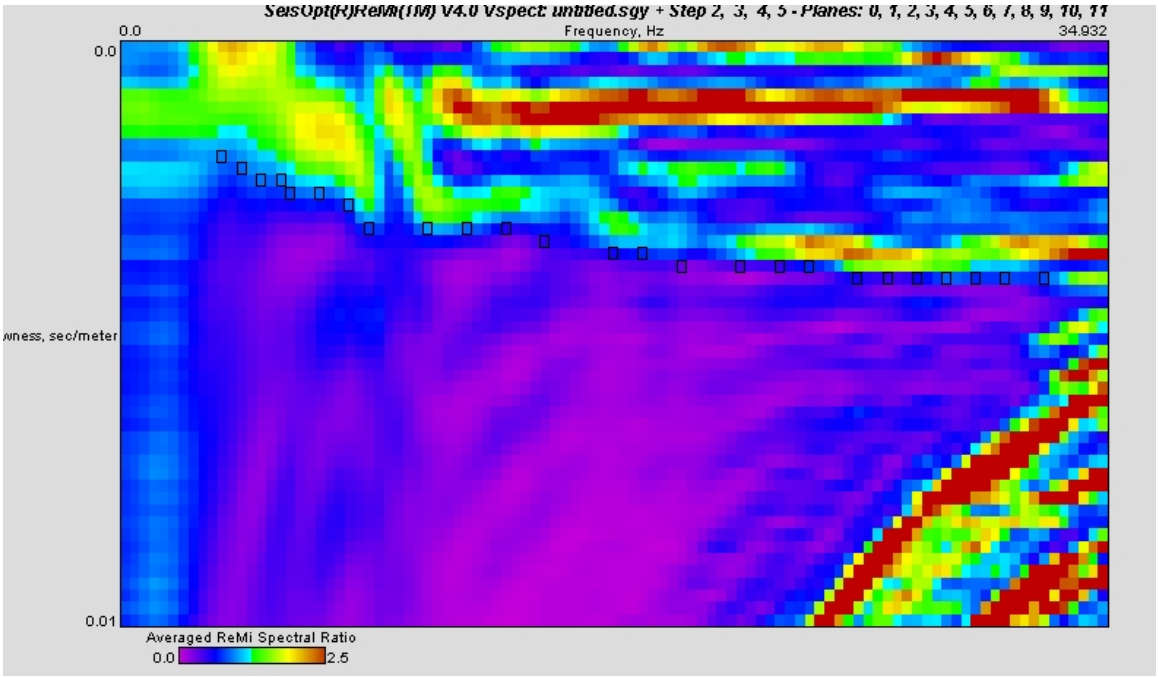

Figure 34. Shown above is the p-f spectrum with picks made along the high amplitude dispersion trend for the first profile in Zone 1.

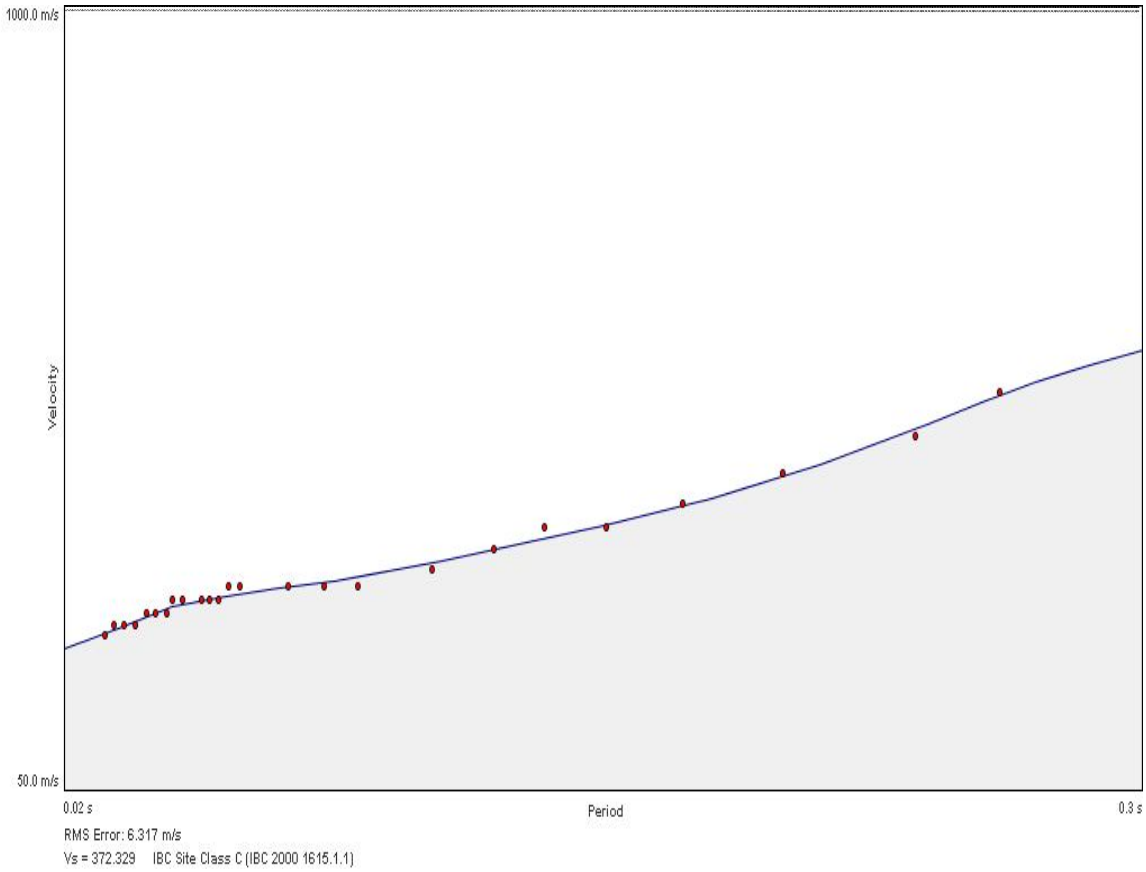

Figure 35. Dispersion curve for the first profile in Zone 1, where the Vs30 is 372 m/s, with a site classification of C. The RMS error is 6.317.

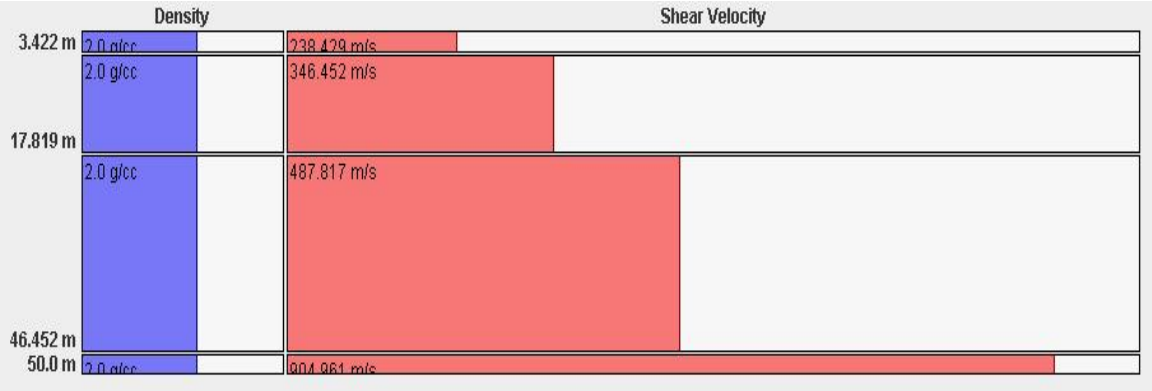

Figure 36. A velocity model for the first profile in Zone 1 showing different layers and shear velocities.

Zone 2 is located just to the east of the University and consists of eight profiles (Figure 37). Table 2 lists the average shear wave velocities and site classifications where four of the profiles have C site classifications with velocities ranging from 453 m/s to 553 m/s, and the other four profiles have D site classifications with average velocities ranging from 330 m/s to 366 m/s. Figure 38 depicts a p-f spectrum for the third profile in Zone 2. Shown in Figure 39 is the dispersion curve for profile 3 found within the alluvial wash unit. Figure 40 shows a velocity model is having three stratigraphic layers. The first layer has a thickness of 5.2 m with a velocity of 220.899 m/s, the second layer has a thickness of 14.9 m with a velocity of 304 m/s, and the third layer has a thickness of 29.8 m with a velocity of 687 m/s. Profile 2 has an average Vs30 of 346 m/s and a site classification of D.

Figure 37. Zone 2 containing eight profiles.

TABLE 3. ZONE TWO PROFILE DATA

Profile #	Line Length (meters)	Geophone Spacing (meters)	Vs30 (m/s)	Site Classification	Latitude	Longitude
1	57.5	2.5	453	C	34°11'0.42"N	117°20'20.43"W
2	57.5	2.5	366	D	34°10'56.30"N	117°20'24.60"W
3	69	3	336	D	34°10'53.27"N	117°20'27.22"W
4	69	3	427	C	34°10'50.29"N	117°20'48.51"W
5	69	3	453	C	34°11'14.76"N	117°21'0.42"W
6	69	3	346	D	34°11'25.89"N	117°20'44.91"W
7	69	3	330	D	34°11'30.14"N	117°20'42.62"W
8	69	3	553	C	34°12'0.93"N	117°20'9.97"W

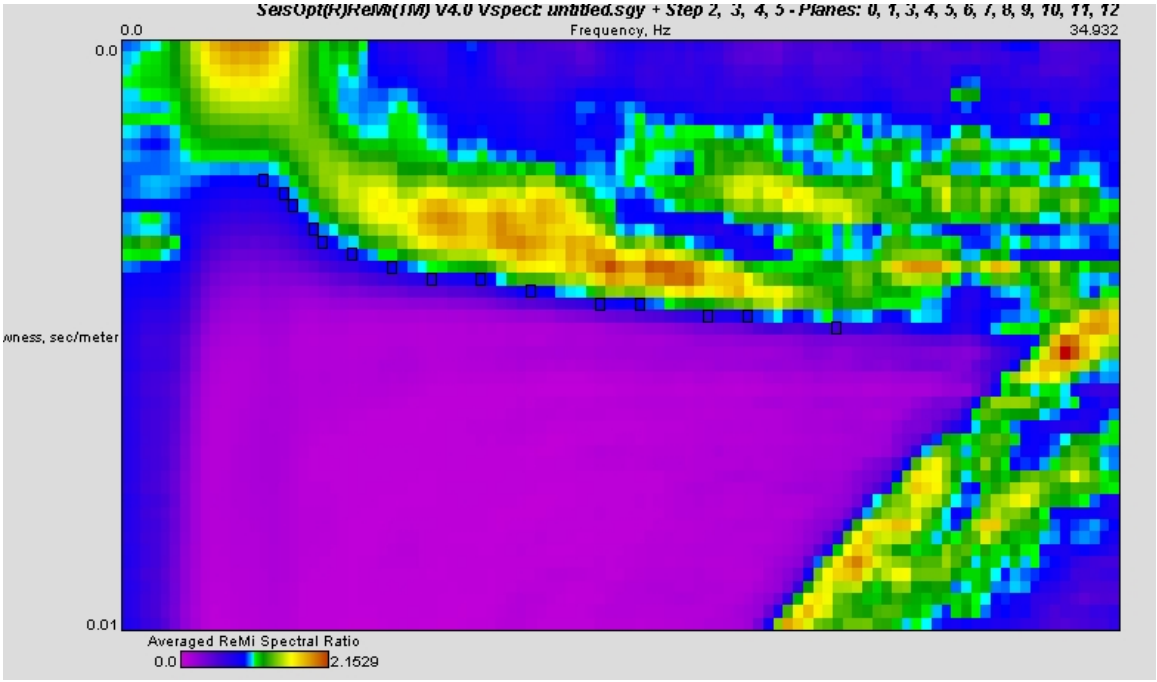

Figure 38. A p-f spectrum with picks along the high amplitude dispersion trend for the third profile of Zone 2.

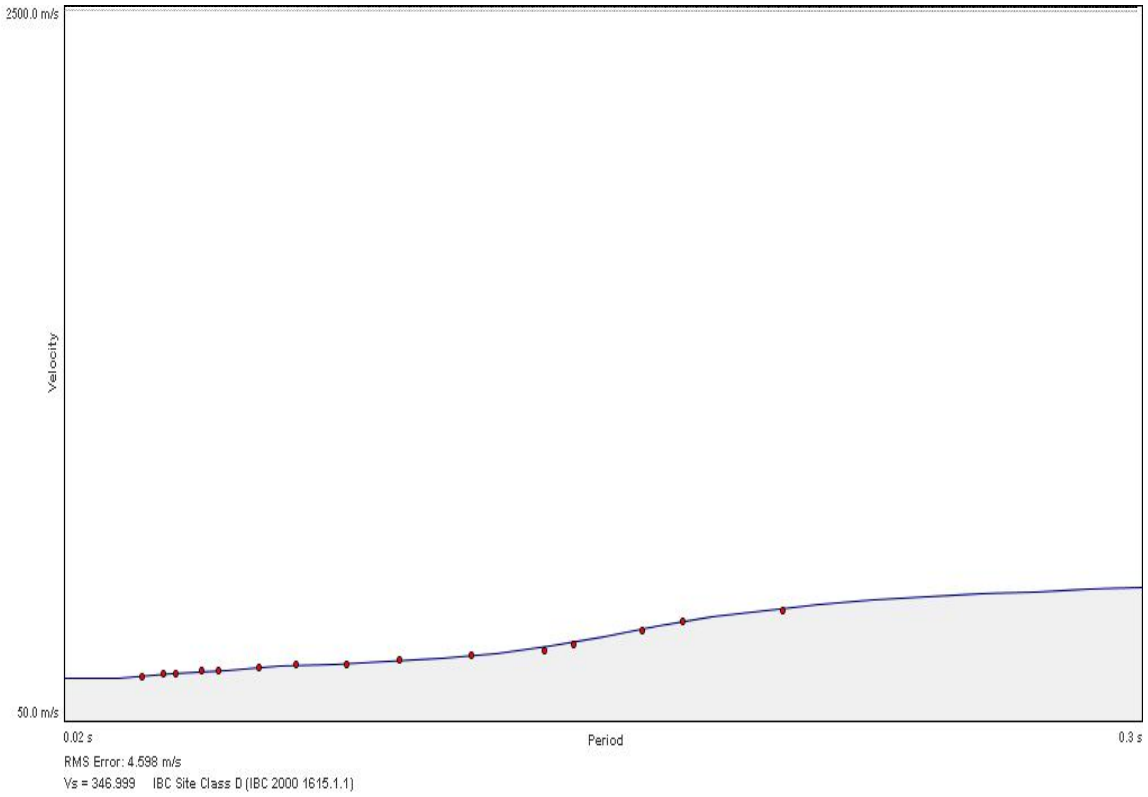

Figure 39. The dispersion curve for the third profile of Zone 2 with an average Vs30 of 346 m/s and a site classification of D. The RMS error is 4.598.

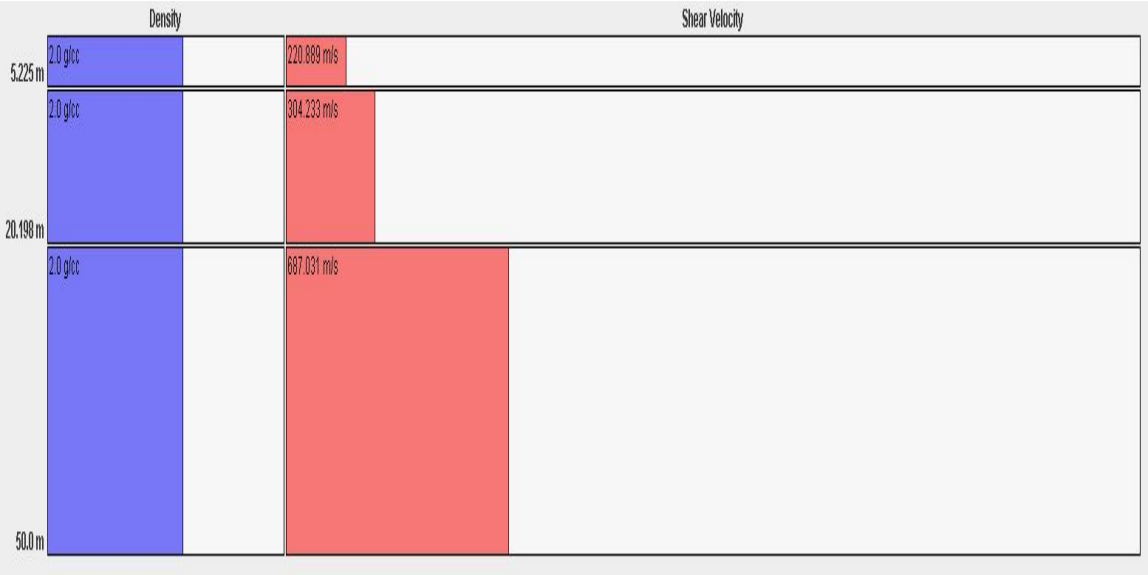

Figure 40. A velocity model showing three stratigraphic layers with varying thickness and shear velocity values for the third profile of Zone 2.

Zone 3 is located to the west of Zone 2, as shown in Figure 41, containing twelve velocity profiles, eleven of which have a C site classification, with average shear velocities ranging from 370 m/s to 474 m/s. One profile has a site classification of D, with a velocity of 366 m/s. A p-f spectrum and dispersion curve for profile 2 is depicted in Figure 42 and Figure 43, and in Figure 44, a velocity model is reproduced having four stratigraphic layers. The first layer has a thickness of 7.4 m with a velocity of 232 m/s, the second layer has a thickness of 12.8 m with a velocity of 455 m/s, the third layer has a thickness of 2.3 m with a velocity of 678 m/s, and the fourth layer has a thickness of 27.3 m with a velocity of 855 m/s.

Figure 41. Zone 3 containing twelve profiles.

TABLE 4. ZONE THREE PROFILE DATA

Profile #	Line Length (meters)	Geophone Spacing (meters)	Vs30 (m/s)	Site Classification	Latitude	Longitude
1	69	3	429	C	34°11'18.45"N	117°21'7.12"W
2	69	3	463	C	34°11'32.25"N	117°21'36.94"W
3	69	3	418	C	34°11'36.73"N	117°21'50.21"W
4	69	3	366	D	34°11'47.78"N	117°21'28.10"W
5	69	3	399	C	34°11'53.87"N	117°21'16.59"W
6	69	3	384	C	34°12'10.48"N	117°21'14.71"W
7	69	3	412	C	34°12'2.76"N	117°21'33.67"W
8	69	3	441	C	34°11'52.47"N	117°21'48.88"W
9	69	3	370	C	34°11'59.37"N	117°21'59.35"W
10	69	3	393	C	34°12'13.59"N	117°22'1.06"W
11	69	3	403	C	34°12'1.22"N	117°22'16.8" W
12	69	3	474	C	34°12'6.95"N	117°22'29.03"W

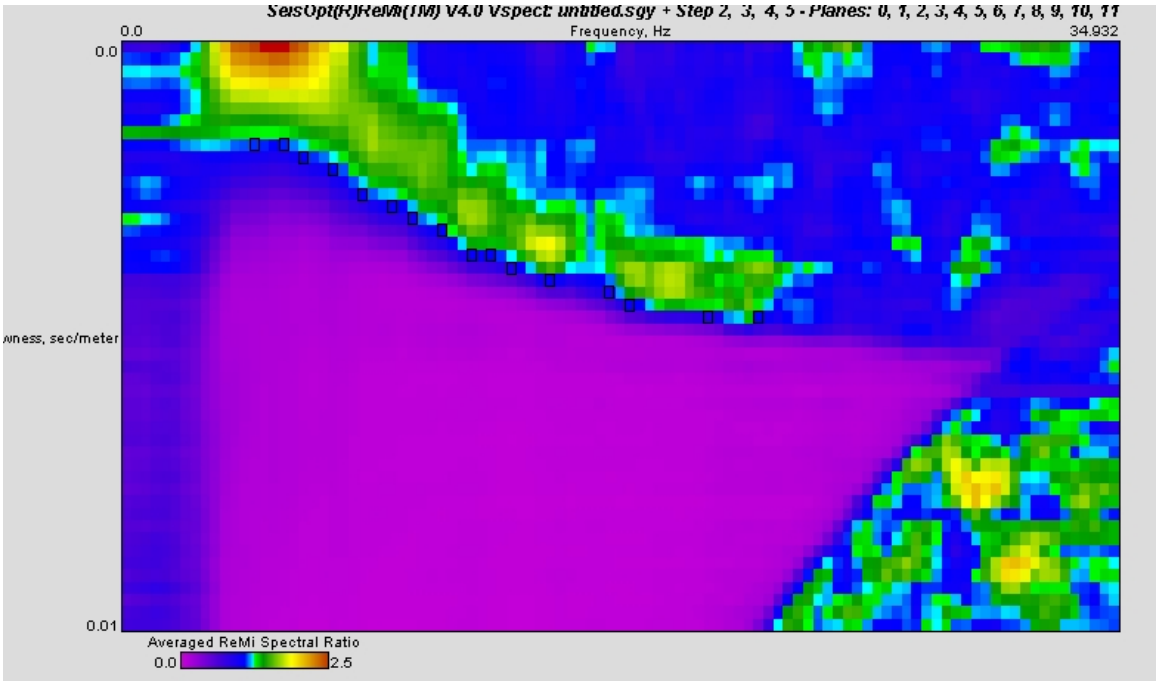

Figure 42. A p-f spectrum with picks along the high amplitude dispersion trend for the second profile of Zone 3.

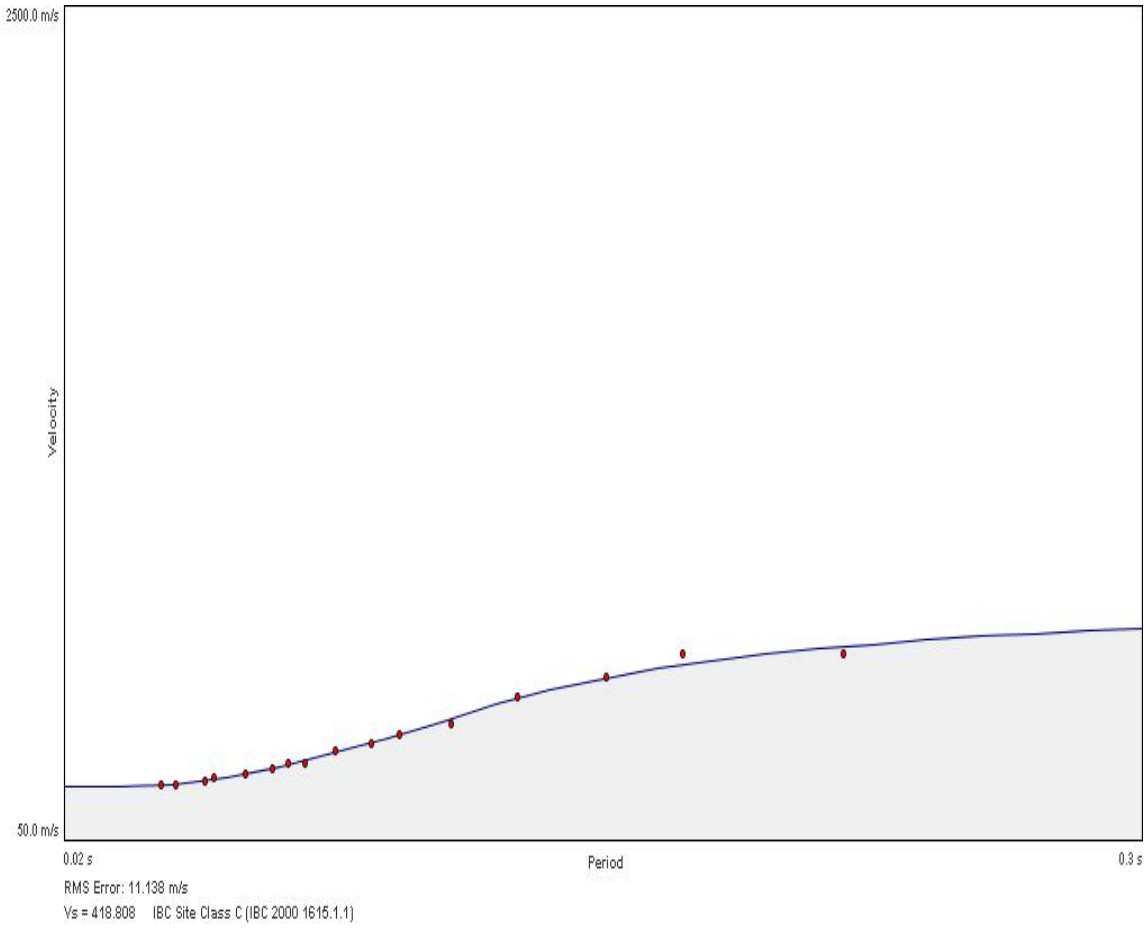

Figure 43. A dispersion curve showing an average Vs30 of 418 m/s and a site classification of C for the second profile of Zone 3. The RMS error is 11.138.

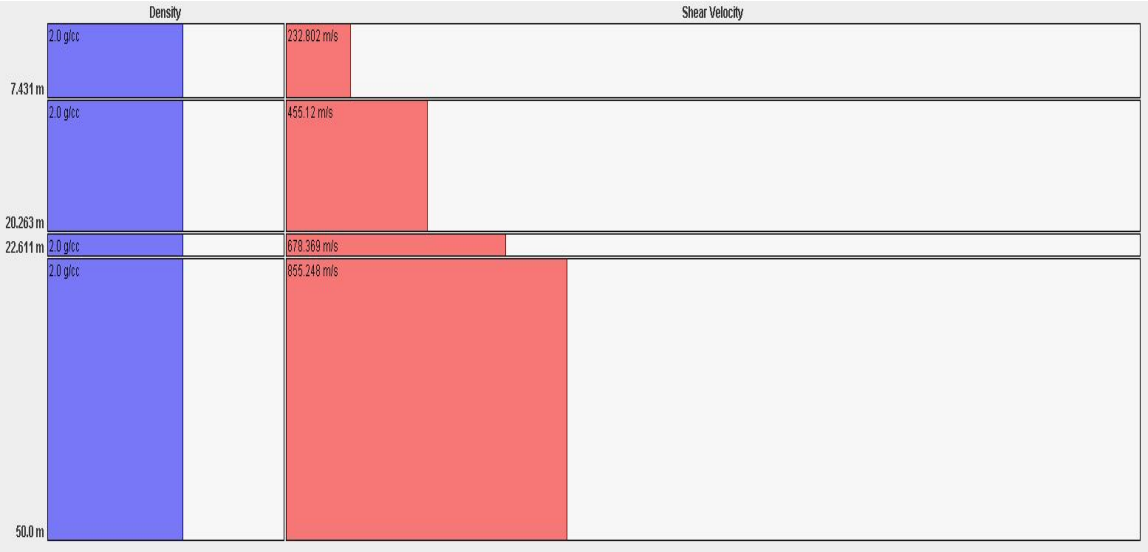

Figure 44. A velocity model depicting four layers, each with varying shear velocity values for the second profile of Zone 3.

Data Interpretation

Using the generated shear wave velocity values within the project area, several analyses were conducted. In Figure 45, Vs30 values were correlated with geologic units. This analysis provides a visual perspective as to where profiles were located within varying geologic units across the project area. This is shown in Figure 46, where geologic unit frequency is illustrated. Unit 3 young alluvial fan deposits (Qwf_3), unit 5 young alluvial fan deposits (Qwf_5) and young alluvial valley deposits (Qya_3) have the highest frequency of coincidence accounting for 21 of the 30 profiles.

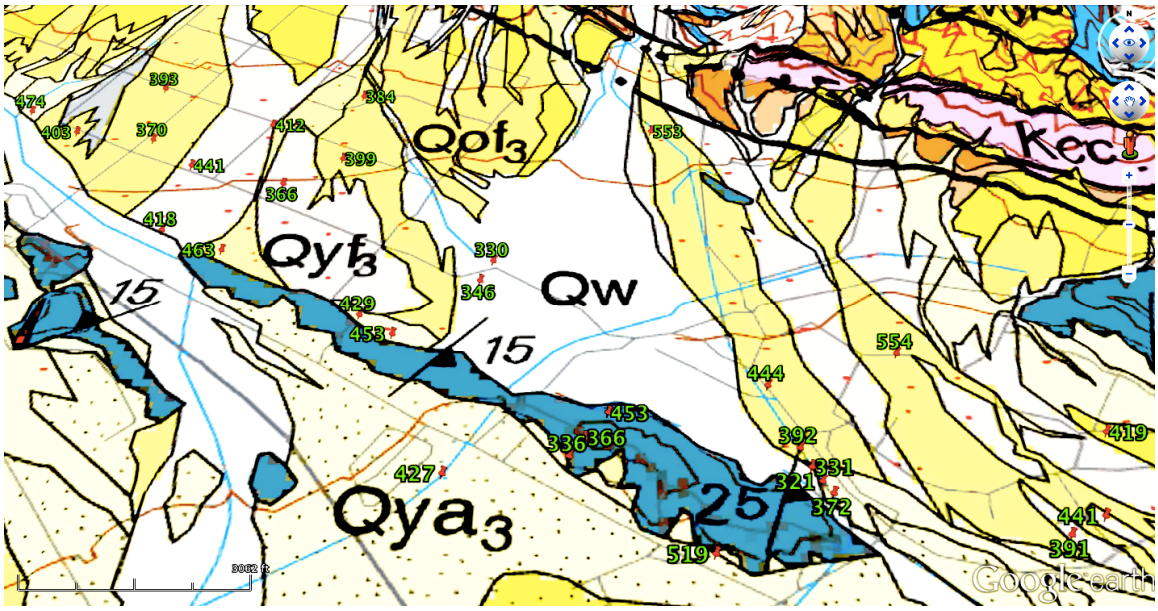

Figure 45. Map containing geologic units and shear wave velocity values acquired within the project area. 30 velocity profiles were constructed within various geologic deposits: very young wash deposits (Qw), unit 1 young alluvial fan deposits (Qyf_1), unit 3 young alluvial fan deposits (Qyf_3), unit 5 young alluvial fan deposits (Qwf_5), unit 3 young alluvial valley deposits (Qya_3) and Pelona Schist units (Mzps) (Morton and Miller, 2006).

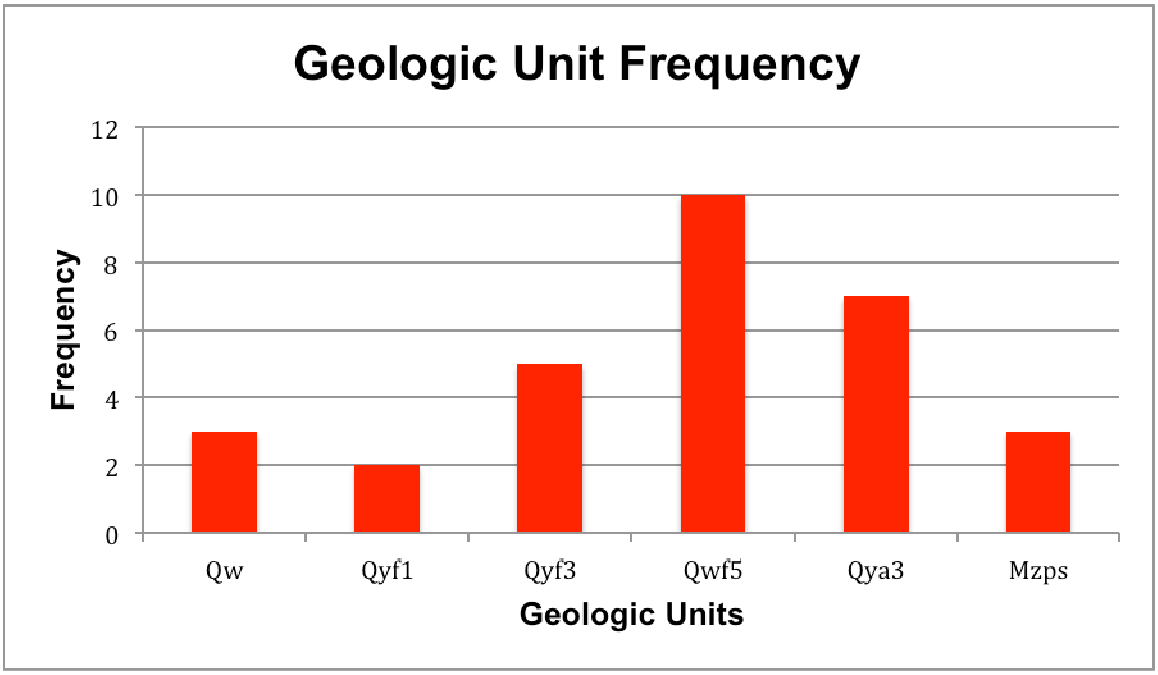

Figure 46. The frequency of coincidence for different geologic units and velocity profiles, where the x-axis is the observed geologic unit and the y-axis is the observed frequency. The geologic units are: very young wash deposits (Qw), unit 1 young alluvial fan deposits (Qyf_1), unit 3 young alluvial fan deposits (Qyf_3), unit 5 young alluvial fan deposits (Qwf_5), unit 3 young alluvial valley deposits (Qya_3) and Pelona Schist units (Mzps). Unit 3 young alluvial fan deposits (Qwf_3), unit 5 young alluvial fan deposits (Qwf_5) and young alluvial valley deposits (Qya_3) have the highest frequency of occurrence.

The geologic units with least representation within the project area are very young wash deposits encompassing three profiles, unit 1 young alluvial fan deposits encompassing two profiles and Pelona Schist bedrock containing three profiles. The primary reason these deposits were under-represented during data acquisition is that few available areas, within aforementioned geologic units, generated adequate seismic noise. A frequency histogram was constructed to show varying Vs30 ranges across the project area (Figure 47). Figure 48 depicts a cumulative frequency graph for the project region. It provides a probabilistic

analysis for observed shear wave velocities where the: lower quartile is 370.5 m/s, median is 407.5 m/s, upper quartile is 443.2 m/s, interquartile range is 72.7 m/s, upper fence is 552.3 m/s and lower fence is 261.3 m/s. Because the upper fence is 552.375 m/s there are two outliers within the data where shear wave velocity values are 554 m/s, and 553 m/s.

Because unit 5 young alluvial fan deposits and unit 3 young alluvial valley deposits make up the majority of the data collected in the project area, cumulative frequency graphs were constructed to individually analyze both units. Figure 49 depicts a cumulative frequency graph for velocities gathered within unit 5 young alluvial fan deposits where the: lower quartile is 392.2 m/s, median is 401 m/s, upper quartile is 458.2 m/s, interquartile range is 66 m/s, upper fence (maximum range limit) is 557.2 m/s and lower fence (minimum range limit) is 293.2 m/s. Figure 50 shows the cumulative frequency for velocities within the unit 3 young alluvial valley deposits where the: lower quartile is 399.5 m/s, median is 429 m/s, upper quartile is 463.5 m/s, interquartile range is 64 m/s, upper fence is 559.5 m/s and lower fence is 303.5 m/s. For all cumulative frequency distribution plots, there is a large interquartile range, which signifies that the data is widely spread from the median, suggesting large variability within the data sets. This variability is attributed to data collection in the field from several different locations.

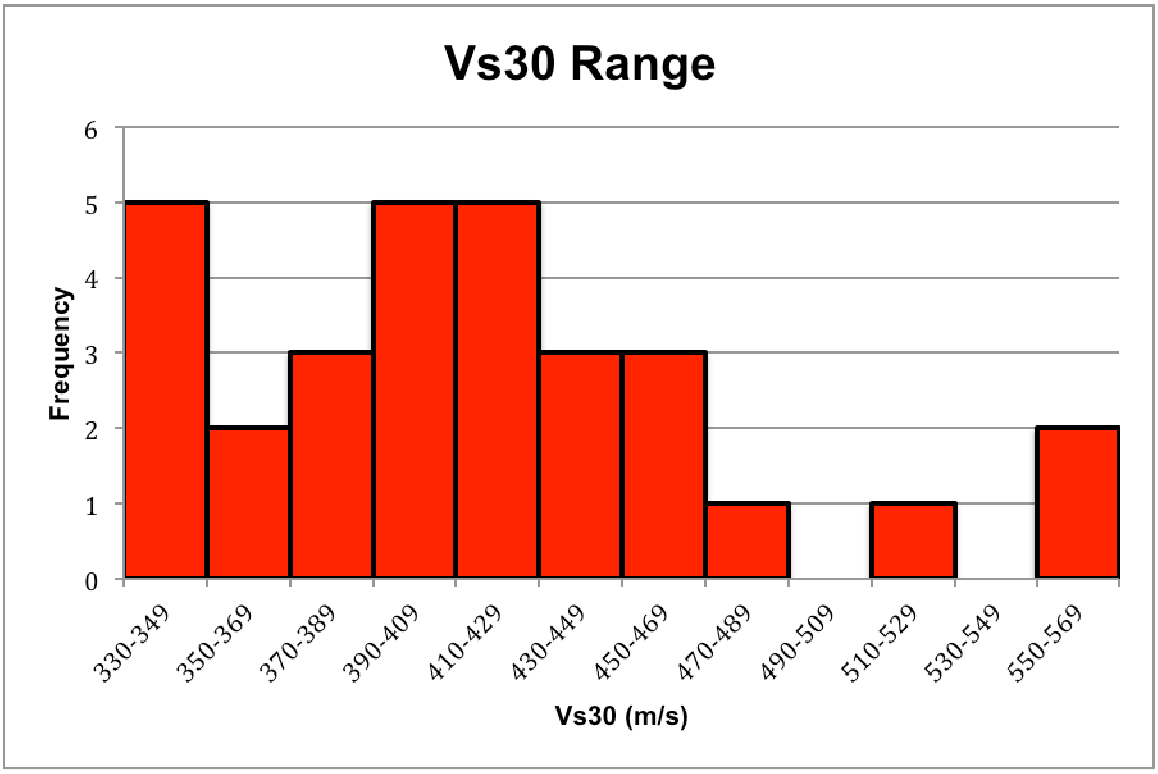

Figure 47. Histogram depicting ranges of Vs30 throughout the project area. The x-axis is Vs30 and y-axis is frequency. Velocity ranges of 330-349 m/s, 390-409 m/s and 410-429 m/s are observed at a higher frequency than other velocity ranges.

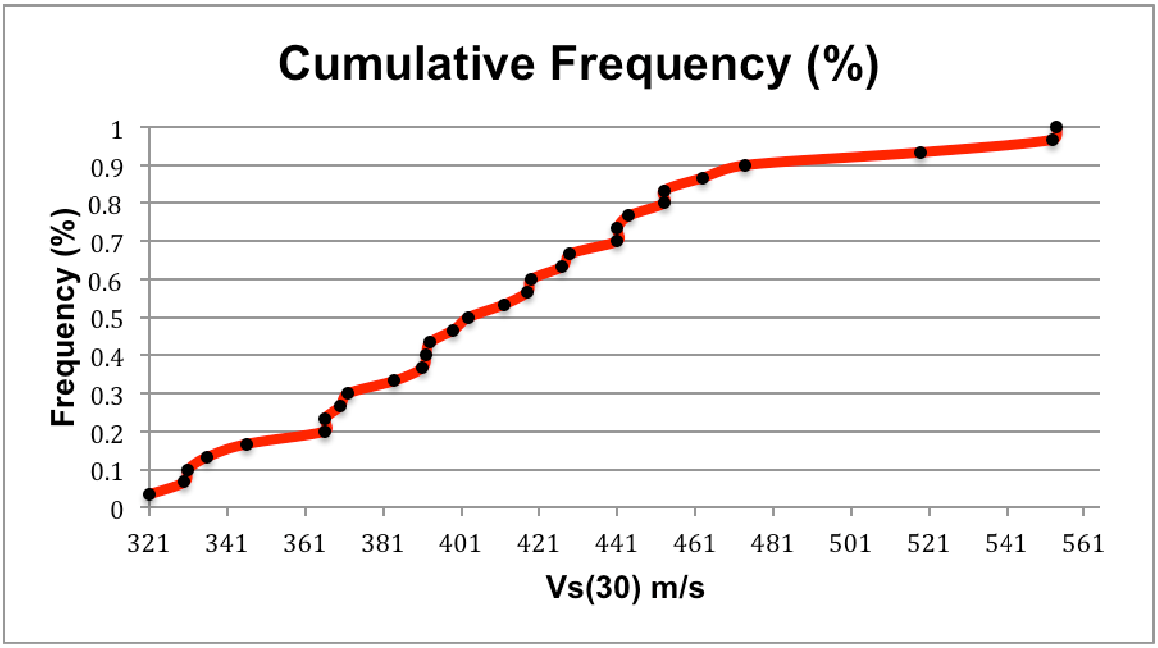

Figure 48. Cumulative frequency plot depicting the probablility of observing specific shear velocities within the project area. The x-axis is Vs30 and y-axis is frequency.

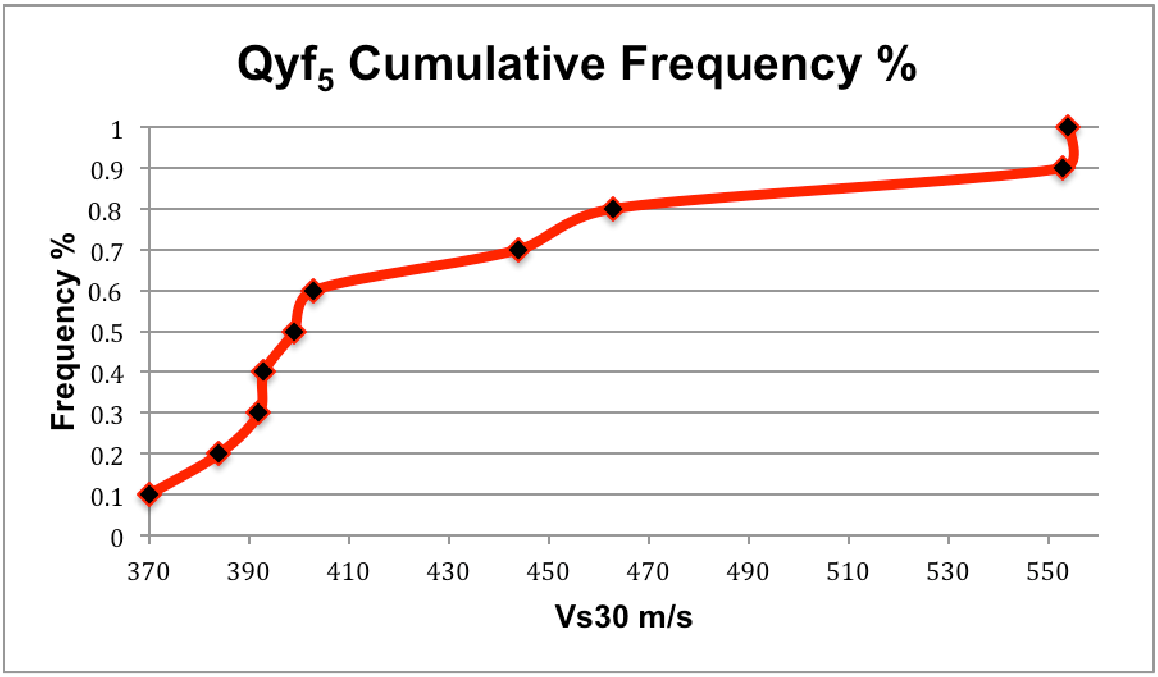

Figure 49. Qyf_5 cumulative frequency plot depicting the probablility of observing specific shear velocities within the unit 5 young alluvial fan deposit. The x-axis is Vs30 and y-axis is frequency.

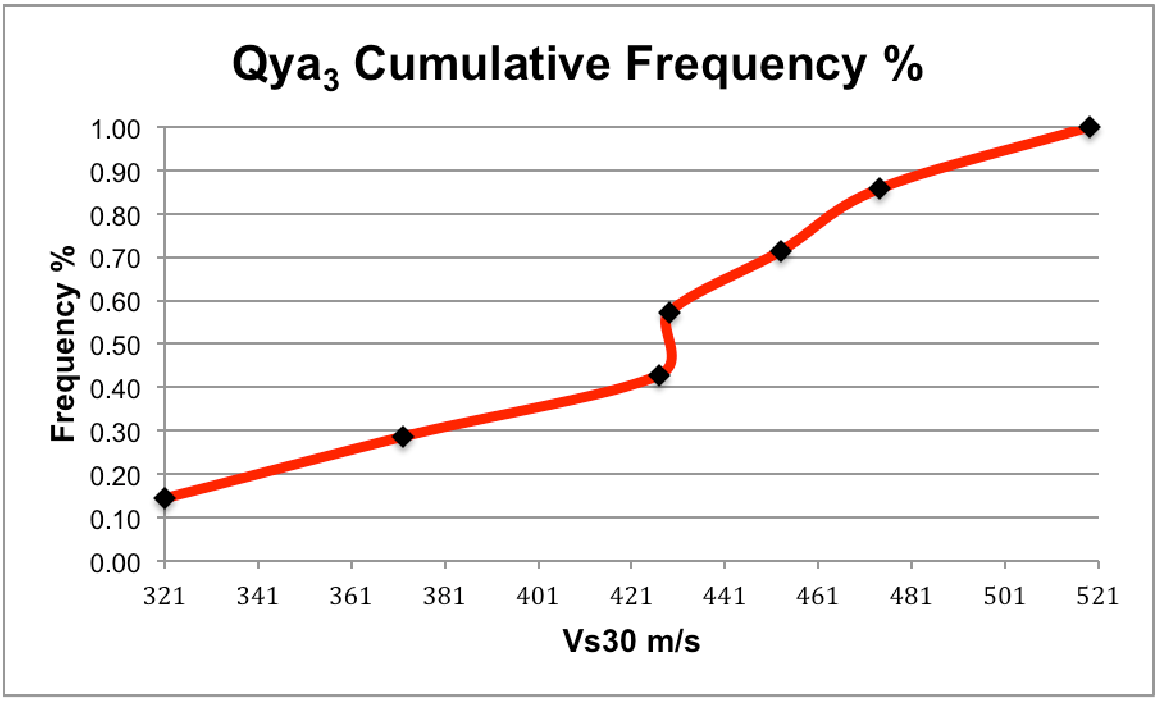

Figure 50. Qya_3 cumulative frequency plot depicting the probablility of observing specific shear velocities in the young alluvial valley deposit geologic unit. The x-axis is Vs30 and y-axis is frequency.

A microzonation contour map was constructed for the project area to show a trend of shear wave velocities from an aerial view (Figure 51). The map depicts all profiles within the project area and their velocities. The color blue represents low velocity areas (300-400 m/s), purple, intermediate velocities (400-500 m/s) and violet, high velocities (500-600 m/s). The red line to the north is the San Andreas Fault. The only apparent trend shown is in the northeastern section of the map, where velocities increase proximal to the San Bernardino Mountains. Based upon this trend, it is assumed that sediment for the top 30 m of the subsurface is relatively compact closer to the mountains compared to distal locations. Shear wave velocity values are directly influenced by sediment

compaction as outlined in NEHRP site classification standards (Table 1). Aside from this, few patterns are present regarding where low or high shear wave velocities are observed. As expected, this indicates that surface geology does not necessarily determine specific shear wave velocities. The lack of patterns may have been attributed to: near surface conditions skewing results (e.g., geophones inserted in hard vs. softer rock and/or the proximity to the water table), a change in geology at depth, and possible inaccuracies of the geologic map. Well logs, such as sonic and density, would be excellent tools to determine specific rock types at depth, but unfortunately were not accessible to compare and corroborate results.

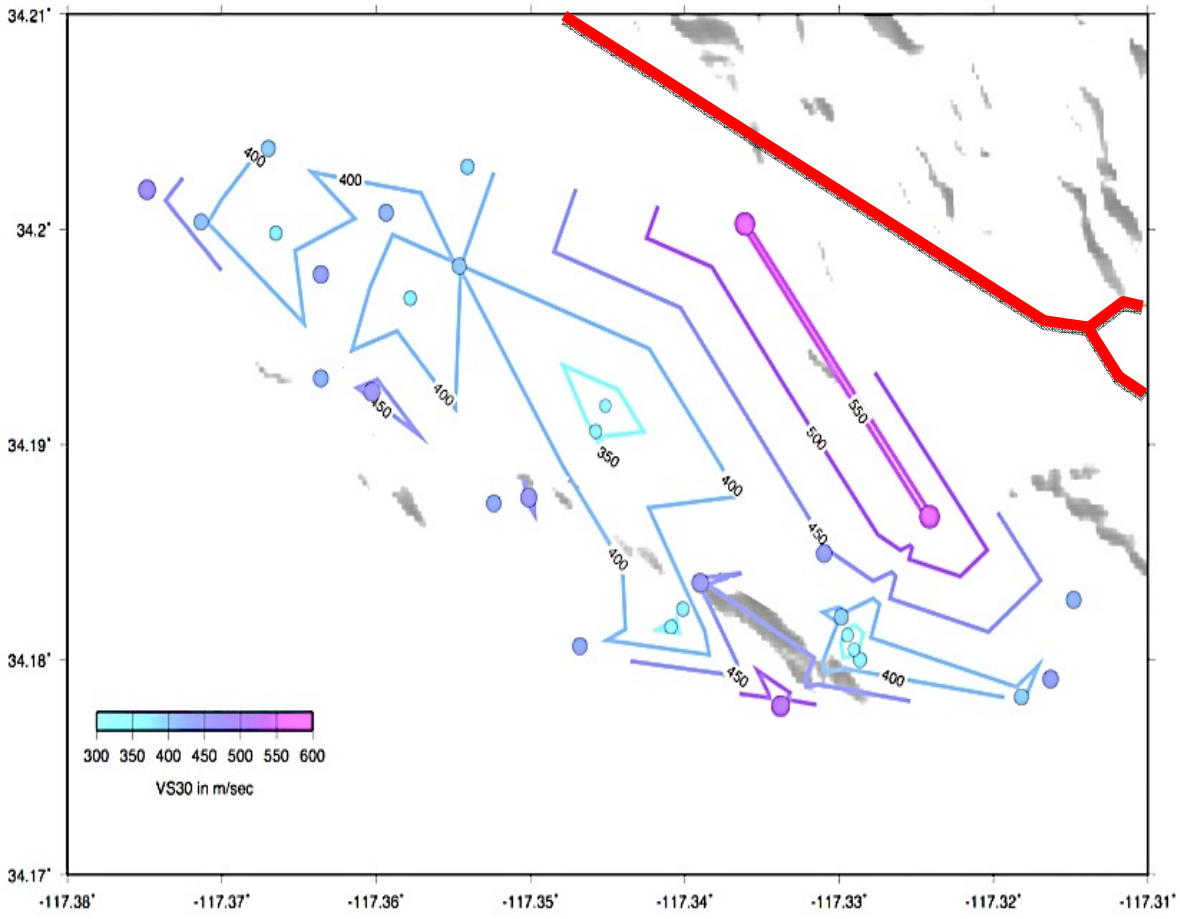

Figure 51. Microzonation contour map of velocity values in the project area where the x and y axis are decimal degree coordinates. Blue indicates low velocity and violet, higher velocity values. The red line represents the San Andreas Fault. North is at the top of the figure.

CHAPTER SEVEN

CONCLUSIONS

Lessons Learned

Identifying areas of seismic hazard is a benefit to the community of San Bernardino. Based upon the findings of this study, there are areas of concern regarding seismic hazards. Seven locations that were analyzed received a site classification of D. Structures built in these locations possess an increased risk for potential failure during earthquakes, especially when considering their close proximity to the San Andreas and San Jacinto Fault zones. Surface geology did not prove as an effective indicator for Vs30 as previously thought. This is based upon the variation of layering in the several stratigraphic velocity models for different areas within a two to three mile proximity to one another. In addition, in areas where surface geology is the same, average shear wave velocities varied. This was evident by observing shear wave velocity values with geologic units in Figure 45 and by the lack of identifiable trends found within the microzonation map generated. Therefore, when generating microzonation maps for this area or surrounding areas, detailed seismic investigations are required because the geologic map cannot be used as a proxy.

Several important pieces of information were learned with regard to the deployment of the ReMi technique. For example, two types of seismic sources were utilized for acquiring Rayleigh wave arrivals. The first was automobile

traffic on roads, and the second was that from the Devils Canyon hydroelectric power plant where seismic wave acquisition was successful at a distance of 200+ meters from the seismic source. This has implications about the range of efficacy of the technique based upon the strength of a seismic source. There were a few situations where seismic profiles were redeployed due to the poor quality of field seismograms and p-f spectra from seismic records acquired. This may have been due to the coupling of the geophones to the ground, or a product of a weak seismic source leading to low resolution data acquisition. Another challenge encountered in the field included the lack of ambient seismic noise during times of decreased automobile traffic on the roads after data collection had already commenced. To increase the efficiency of the study, it would be best to conduct experiments during times of high traffic, i.e., in the morning or early evening during rush hour, to maximize potential ambient seismic noise.

Work for the Future

For future investigations, the study area should be expanded to include increased profile deployment within Pelona Schist exposures, very young wash deposits and unit 1 young alluvial fan deposits. In addition, surrounding geologic units that were not in the initial study should be incorporated in an expanded investigation to better classify potential seismic hazards in the region. Experimenting with wave arrivals from different ambient sources, e.g. trains, would also be valuable. Although logs from ground water wells are available upon request from the owners, those data are confidential and cannot be used

within publications without consent. To provide a publically accessible database, the state of California should authorize an investigation where core sampling is conducted throughout the state in areas with known seismic hazards. Such a study would provide a tangible correlation standard, where results attained from stratigraphic velocity models could be compared against a physical lithologic sample.

The results gained thus far provide a solid footing for future work to be done in seismic hazard assessments in the San Bernardino area. The data from this study are available to the public and governing bodies, to highlight the risk of geologic hazards. Best practices for constructing homes and commercial structures should recognize the potential impact geologic hazards pose to the safety of the community.

REFERENCES CITED

Aki, K., 1957, Space and time spectra of stationary stochastic waves, with special reference to microtremors: Bulletin of the Earthquake Research Institute, v. 35, p. 415-456.

Alquist, A., and Priolo, P., 1972, Alquist-Priolo Geologic Hazard Zones Act: State of California Senate Bill SB 520 (enacted December 22, 1972, effective from March 7, 1973): California Public Resources Code, Division 2, Chapter 7.5.

Boore, D.M. and Brown, L.T., 1998, Comparing shear-wave velocity profiles from inversion of surface-wave phase velocities with down hole measurements: systematic differences between the CXW method and down hole measurements at six USC strong-motion sites: Seismological Research Letters, v. 69, p. 222-229.

Borcherdt, R. D., 1975, Studies for seismic zonation of the San Francisco Bay region, U.S. Geological Survey Professional Paper 941-A, p. 102.

Building Seismic Safety Council, 2003, NEHRP Recommended provisions for seismic regulations for new buildings and other structures, Part 1: Provisions, FEMA 368, Federal Emergency Management Agency, Washington, D.C., p. 1-288.

Chester, F.M., 1993, Internal structure and weakening mechanisms of the San Andreas fault: Journal of Geophysical Research, v. 98, p. 771-786.

Duke, C.M., 1969, Techniques for field measurement of shear wave velocity in soils, in Proceedings, 4th World Conference on Earthquake Engineering, Santiago, Chile, p. 39-54.

FEMA, 1997, NEHRP recommended provisions for seismic regulations for new buildings and other structures, NEHRP, p. 1-343.

Freed, A.M. and Lin, J., 2002, Accelerated stress buildup on the southern San Andreas fault and surrounding regions caused by Mojave Desert earthquakes: Geology, v. 30, p. 571-574

Heisey, J. S., Stokoe II, K. H., and Meyer, A. H., 1982, Moduli of pavement systems from spectral analysis of surface waves: Transportation Research Record No. 852, p. 22-31.

Holzer, T.L., Padovani, A.C., Bennett, M.J., Noce, T.E., and Tinsley, J.C., 2005, Mapping NEHRP Vs30 site classes: Earthquake Spectra, v. 21, p. 1-18.

Horike, M., 1985, Inversion of phase velocity of long-period microtremors to the s-wave velocity structure down to the basement in urbanized areas: Journal of Physics of the Earth. v. 33, p. 59-96.

Hoversten, G.M., Milligan, P., Byun, J., Washbourne, J., Knauer, L.C., and Harness, P., 2004, Crosswell electromagnetic and seismic imaging: An examination of coincident surveys at a steam flood project: Geophysics, v. 69, p. 406-414.

Jennings, C.W., 1994, Fault activity map of California and adjacent areas with location and ages of recent volcanic eruptions: California Division of Mines and Geology, California Geologic Data Map Series Map No. 6.

Jones, L.M., 1995, Putting down roots in earthquake country, SCEC Special Publication: Los Angeles, CA, p. 22-23.

Lawson, A.C., Leuschner, A.O, Gilbert, G.K., Davidson, G., Reid, H.F., Burkhalter, C., Branner, J.C., and Campbell, W.W., 1969, The California earthquake of April 18, 1906, Carnegie Institution of Washington, p. 1-451.

Louie, J.N., 2001, Shear-Wave Velocity to 100 Meters depth from refraction microtremor arrays: Bulletin of the Seismological Society of America, v. 91, p. 347-364.

Marion, B., 2014, Cross-well Imaging offers higher resolution: The American Oil and Gas Reporter, p. 1-5.

Morton, D., and Miller, F.K., 2006, Preliminary geologic map of the San Bernardino North 30' by 60’ quadrangle, California: U.S. Geological Survey Open-File Report 03-293, 1 map, 194 p., http://pubs.usgs.gov/of/2003/of03-293/

Mount, V.S., 1987, State of stress near the San Andreas fault: Implications for wrench tectonics: Geology, v. 15, p. 1143-1146.

O’Rourke, T.D., 1992, The Loma Prieta, California, earthquake of October 17, 1989- Marina District: U.S. Geological Survey Professional Paper, 1551-F, p. 1-195.

Optim LLC, 2006, User’s manual SeisOpt ReMi version 3.0: Optim Software & Data Solutions.

Park, C.B., Miller, R.D., and Xia, J., 1997, Multichannel analysis of surface waves: Kansas Geological Survey Open-File Report 97-10, p. 1-26.

Park, C.B., Miller, R.D., and Xia, J., 1999, Multichannel analysis of surface waves: Geophysics, v. 63, p. 800-808.

Petersen, M.D. and Wesnousky, S.G., 1994, Fault slip rates and earthquake histories for active faults in southern California: Bulletin of the Seismological Society of America, v. 84, p. 1608-1649.

Rosenblad, B. L., Rathje, E. M., and Stokoe, K. H., 2002, Shear wave velocity profiling by SASW method at selected strong-motion stations in Turkey: Pacific Earthquake Engineering Research Center Site Response Report No. 2A02a, p. 1-53.

Roser, J., and Gosar, A., 2010, The determination of Vs30 for seismic ground classification in the Ljubljana area, Slovenia: ACTA Geotechnica Slovenia, v. 7, p. 60-76.

Schulz, S.S. and Wallace, R.E., 2013, The San Andreas fault, USGS, Online Version: http://pubs.usgs.gov/gip/earthq3/endnotes.html (August 2014).

Segall, P., 1990, Loma Prieta earthquake: Geophysics News, v. 29, p. 9-10.

Stein, R. S., King, G.C.P., and Lin, J., 1992, Change in failure stress on the southern San Andreas fault system caused by the 1992 magnitude 7.4 Landers earthquake: Science, v. 258, p. 1328-1332.

Stephenson, W.J., Williams, R.A., Odum, J.K., and Worley, D.M., 2005, Comparison of ReMi, and MASW shear-wave velocity techniques with the CCOC borehole to 100 m, Santa Clara Valley, in blind comparisons of shear-wave velocities at Closely-Spaced sites in San Jose, California, Asten, M.W. and Boore, D.M., eds., U.S. Geological Survey Open-File Report 2005-1169, p. 1-6.